GLOBAL BIOGEOCHEMICAL CYCLES, VOL. 10, NO. 2, PAGES 361–382, JUNE 1996

The role of the vertical fluxes of particulate organic matter and calcite in the oceanic carbon cycle: Studies using an ocean biogeochemical general circulation model

Yasuhiro Yamanaka

Center for Climate System Research, University of Tokyo, Tokyo, Japan

Eiichi Tajika

Geological Institute, School of Science, University of Tokyo, Tokyo, Japan

Abstract. Distributions of chemical tracers in the world ocean are well reproduced in an ocean general circulation model which includes biogeochemical processes (biogeochemical general circulation model, B-GCM). The difference in concentration of tracers between the surface and the deep water depends not only on the export production but also on the remineralization depth. Case studies changing the vertical profile of particulate organic matter (POM) flux and the export production show that the phosphate distribution can be reproduced only when the vertical profile of POM flux observed by sediment traps is used. The export production consistent with the observed distribution of phosphate is estimated to be about 10 GtC/yr. Case studies changing the vertical profile of calcite flux and the rain ratio, a ratio of production rate of calcite against that of particulate organic carbon (POC), show that the rain ratio should be smaller than the widely used value of 0.25. The rain ratio consistent with the observed distribution of alkalinity is estimated to be 0.08 to approximately 0.10. This value can be easily understood in a two-box model where the difference of remineralization depth between POC and calcite is taken into account.

1. Introduction

The marine carbon cycle has an important role in controlling the concentration of atmospheric CO_2. It has been widely studied by using various models such as simple box models and three-dimensional general circulation models.

A pioneering study on the ocean carbon cycle with an ocean general circulation model which is extended to include biogeochemical processes was made by *Bacastow and Maier-Reimer* [1990]. They showed that the distributions of oceanic tracers, such as phosphate, dissolved oxygen, alkalinity, total CO_2, and $\delta^{13}C$ can be roughly reproduced in their model, although there were some features which are compared poorly with the observations (for example, the depth of phosphate maximum was too deep). Recently, *Maier-Reimer* [1993] improved their model, and the calculated distributions of tracers have better resemblance with the observation of Geochemical Ocean Sections Study (GEOSECS). *Najjar et al.* [1992] studied phosphate cycling by using their general ocean circulation model, and pointed out that the concentration of phosphate in water under high-productivity areas should be higher and the high productivity is maintained by upwelling of this phosphate-rich water. They called this positive feedback mechanism "nutrient trapping". However, since the thermocline depth was unrealistically deep in their model, the depth of phosphate maximum was also unrealistically deeper than the observed.

Here, the results of simulations with general circulation models are directly compared with observations. In particular, a GCM which is extended to include effects of biogeochemical processes (B-GCM) can deal not only with current field, temperature, and salinity, but also with many biogeochemical tracers such as phosphate and dissolved oxygen. We can obtain much more information about the ocean circulation from the study using B-GCM, as these tracers have been measured extensively by oceanographic expeditions for a long time. Furthermore, the model including isotopes like $\delta^{13}C$ is a

Paper number 96GB00634.
0886-6236/96/96GB-00634$12.00

useful tool to study not only the present ocean but also the paleocean [*Heinze et al.*, 1991]. It is, however, noted that there are several disadvantages in the study with GCMs: it requires computer resources and it is very difficult to interpret the numerical results compared to the study than simple models.

Biological activity also affects distributions of total CO_2 and alkalinity. Carbon in the form of particulate organic carbon (POC) as soft tissue of organisms is produced by biological activity in the surface water. As POC sinks from the surface to the deep layer, the concentration of total CO_2 in the surface water decreases and alkalinity slightly increases (the latter is due to consumption of NO_3^-). As a result, the partial pressure of atmospheric CO_2 decreases. Similarly, carbon in the form of calcium carbonate (mainly as calcite) as hard parts of organisms is also produced by biological activity in the surface water. Calcite sinks from the surface to the deep layer, and the concentration of total CO_2 and alkalinity in the surface water decreases. As a result, the partial pressure of atmospheric CO_2 increases. Both total CO_2 and alkalinity in the deep water are generally higher than those in the surface water, because POC and calcite are remineralized while they are sinking. Ocean circulation brings up the deep water rich in total CO_2, alkalinity, and also nutrients, which are necessary to biological activity, to the surface layer by upwelling and convection. In this way, the atmospheric CO_2 level and the distributions of total CO_2 and alkalinity in the ocean are determined by the balance between the biological activity and the ocean circulation.

As described above, the production and remineralization of POC and calcite affect the carbon cycle in a different way. The ratio of production rate of calcite to that of POC is very important, and it is generally called the "rain ratio". When the rain ratio is large, the partial pressure of CO_2 in the surface water would be high. When it is small, the partial pressure of CO_2 would be low. The rain ratio is estimated to be 0.25 by the two-box model [e.g., *Broecker and Peng*, 1982], and this value has been widely used. However, recent observations provide an estimate of the rain ratio to be a much smaller value of 0.11 to approximately 0.03 [*Takahashi et al.*, 1990]. We will show that the value of the rain ratio should be 0.08 to approximately 0.10.

As shown by *Yamanaka* [1995], the effect of dissolved organic matter (DOM) on the carbon cycle is limited to the surface layer, roughly above the depth of 400m, and the effect of DOM on the distribution of the chemical tracers in the deeper layer below 400m is much weaker than that of POM. We will not treat DOM in this study, because DOM hardly affects the global phosphate distribution, especially in the deep layer. The role of dissolved organic matter in the oceanic carbon cycle is still controversial [*Siegenthaler and Sarmiento*, 1993].

In the next section, the model developed in this study will be described. In section 3, the vertical transport due to the biological pump is discussed by using a simple model. We will show that the smaller value of the rain ratio is obtained by taking into account the depths at which POM and calcite are remineralized. In section 4, the distributions of tracers are obtained for the model with the observed vertical profile of POM flux, and the appropriate rain ratio is presented. In section 5, the case studies changing the bioproduction efficiency, the vertical profile of POM flux, the rain ratio, and calcite flux are made, and the role of these parameters in the carbon cycle is discussed. In the final section, the results are summarized.

2. Model

We develop an ocean biogeochemical general circulation model, which is basically similar to the model of *Bacastow and Maier-Reimer* [1990]. The ocean biogeochemical general circulation model actually makes use of flow fields and distributions of temperature and salinity of the world ocean, which are obtained by the general circulation model.

General Circulation Model

To obtain the circulation in the world ocean, we use the Center for Climate System Research (CCSR) ocean general circulation model. The CCSR model is almost the same as the Geophysical Fluid Dynamics Laboratoty (GFDL) model [*Bryan*, 1969] for the finite difference scheme except that the weighted upcurrent scheme is adopted for the advection terms of temperature and salinity [*Suginohara et al.*, 1991]. The horizontal resolution is four degrees. There are 17 levels in the vertical, whose grid size increases with depth, from 50m for the surface layer to 500m for the deep layers. We adopt a realistic ocean bathymetry, but the Arctic Sea and the Mediterranean Sea are not included.

The model is driven by the wind stress and buoyancy forcing at the sea surface. The wind stress used in our model is taken from the annual mean data set of *Hellerman and Rosenstein* [1983]. As for the buoyancy forcing, temperature and salinity at the sea surface level are restored to the reference values taken from the annually averaged data sets of *Levitus* [1982]. However, since the North Atlantic Deep Water (NADW) becomes weak under the annual mean condition of the sea surface temperature, we take a reference temperature which is 4K cooler than the annual mean condition at 60°N (this corresponds to the midwinter condition) and decreases linearly from 50°N to 60°N. As a result, we obtained the transport of NADW comparable with the observation (see section 4).

Initial conditions are no motion and horizontally uniform distributions of temperature and salinity. After carrying out the time integration for 10,000 years, we obtain flow fields and distributions of temperature and salinity which can be regarded as a steady state.

Biogeochemical General Circulation Model

Prognostic variables and mass conservation. Prognostic variables in our B-GCM are concentrations of atmospheric CO_2, oceanic total CO_2, alkalinity, phosphate, and dissolved oxygen. Concentrations of these tracers are calculated as the forms normalized by salinity of 35 practical salinity unit (psu). The fact that the mixing process of CO_2 in the atmosphere is much faster than that in the ocean allows the atmosphere to be treated as one box.

Carbon 13 is treated as an individual tracer, and hence $^{13}CO_2$ in the atmosphere and total $^{13}CO_2$ in the ocean are also prognostic variables. Although ^{14}C is not dealt with as an individual tracer, we consider it in the form of $\Delta^{14}C$ according to the method of *Toggweiler et al.* [1989].

As will be described, sedimentation processes and river input due to the continental weathering are not included in our model. Therefore, the total amounts of ^{12}C and ^{13}C are conserved in the atmosphere-ocean system. Similarly, the total amounts of phosphate and alkalinity are conserved in the ocean.

Dynamic process. Dynamic processes such as advection and diffusion of tracers in our B-GCM follow an equation similar to that used in the general circulation model:

$$\frac{\partial C}{\partial t} + \boldsymbol{u} \cdot \nabla C = A_{HH}\nabla_H^2 C + A_{HV}\frac{\partial^2 C}{\partial z^2} + S_C, \quad (1)$$

where C represents the concentration of each tracer, S_C represents a source term due to biological process, and $\boldsymbol{u}$ is current velocity. A_{HH} and A_{HV} are horizontal and vertical diffusion coefficients, respectively. We assume the same values for A_{HH} and A_{HV} as those in the circulation model.

Kuo and Veronis [1970] estimated $A_{HH} = 6\times10^2 m^2/s$ from the horizontal distribution of dissolved oxygen in the abyssal layer, although the value on the order of $10^3 \sim 10^4 m^2/s$ is usually adopted in the GCM to avoid numerical instability. We take $A_{HH} = 8 \times 10^2 m^2/s$ in our model. The distributions of tracers are sensitive to the thermocline depth, because most of particulate organic carbon is remineralized at depths shallower than the thermocline. It is well known that the thermocline depth is dependent on A_{HV} [*Bryan*, 1987]. Therefore, it is important to adopt an appropriate value for A_{HV}. In our model, we take $A_{HV} = 0.2 \times 10^{-4} m^2/s$, which is comparable with observations [e.g., *Ledwell et al.*, 1993].

Chemical process and gas exchange. The chemical and biological processes considered in our model are illustrated in Figure 1. The surface partial pressure of carbon dioxide pCO_2 is derived from alkalinity, total CO_2, temperature, and salinity under the condition of chemical equilibrium. Alkalinity is determined in the carbon-borate-water system, where the total amount of borate is given as a linear function of salinity. The apparent dissociation constants for carbon, borate, and water are taken from *Dickson and Millero* [1987], *Johansson and Wedborg* [1979], and *Dickson and Riley* [1979]. The solubility of carbon dioxide is taken from *Weiss* [1974]. Gas exchange of CO_2 through the sea surface is assumed to be proportional to the difference of pCO_2 between the atmosphere and the surface ocean. The gas exchange coefficient is assumed to be globally uniform at $K = 0.06$ mol/(m^2 yr μatm) [*Maier-Reimer*, 1993].

The partial pressure of carbon dioxide in the atmosphere is not locally in equilibrium with that in the ocean. Therefore, we do not consider an equilibrium fractionation factor but consider one-way fractionation factors for carbon exchange from the ocean to the atmosphere and from the atmosphere to the ocean as functions of temperature and concentrations of carbon dioxide, bicarbonate ion, and carbonate ion. The details of treatments of fractionation process of carbon isotope through the gas exchange are described in the appendix.

The concentration of dissolved oxygen in the surface

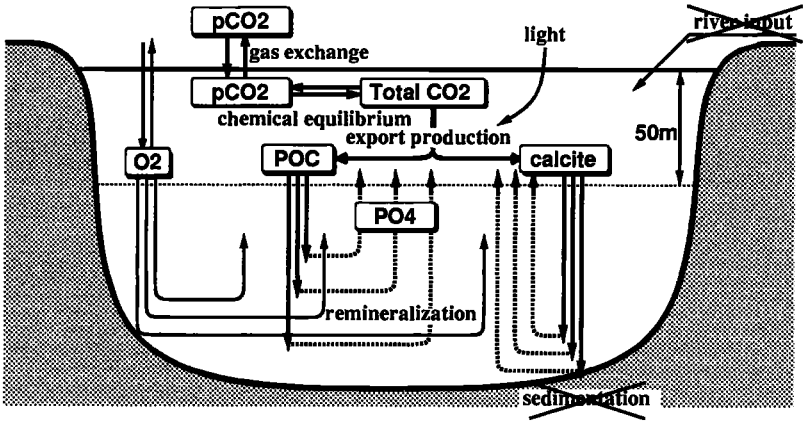

Figure 1. Chemical and biological processes considered in the biogeochemical general circulation model (B-GCM). Processes of sedimentation and river input are not included.

water is restored to be saturation level in a restoring time of 17 days [*Broecker and Peng*, 1982]. The value of saturation is taken from *Weiss* [1970].

Export production. Photosynthesis and hence biological production takes place only in the surface layer of the ocean. Export production EP is firstly considered as a function of phosphate concentration $[PO_4]$ and light factor L_f as follows:

$$EP = rL_f\,[PO_4]\frac{[PO_4]}{h+[PO_4]}\,z_b \qquad (2)$$

where h is a half-saturation constant, r is a proportional factor (we call this "bio-production efficiency"), and z_b is the surface layer depth. The light factor L_f is proportional to an annually averaged solar radiation, which is a simple function of latitude and is normalized to be $0 \le L_f \le 1$. The dependency of phosphate concentration on EP is assumed to follow Michaelis-Menten kinetics [*Maier-Reimer*, 1993]. However, since phosphate concentration in the surface water is usually much larger than the half-saturation constant of 0.02μmol/L [*Maier-Reimer*, 1993], we approximate EP to be a linear function of $L_f[PO_4]$ for simplicity. In this study, we use $r = 0.8$ yr^{-1}, which is obtained by fitting the observed phosphate distribution. The dependency of the observed phosphate distribution and atmospheric CO_2 level on the bioproduction efficiency will be described in section 5.

Composition of POM is assumed to follow the classical Redfield ratio,

$$P : N : C : -O_2 = 1 : 16 : 106 : 138. \qquad (3)$$

As will be discussed in section 3, the value of the rain ratio R, a ratio of production rate of calcite to that of POC, is assumed to be 0.08 in the control case, which is much smaller than 0.25 estimated from the two-box model [e.g., *Broecker and Peng*, 1982]. We also calculate cases changing the rain ratio, $R = 0.06$ through 0.20.

Organisms consume ^{12}C preferentially to ^{13}C to form their soft tissue through photosynthesis. The value of the fractionation factor for this process is assumed to be $-22‰$ [*Tans et al.*, 1993] (the definition for the fractionation factor is given in the appendix). However, when the biota form their hard parts (calcite), the value of the fractionation factor is assumed to be 0‰ [*Tans et al.*, 1993]. This is because the effect of carbon fractionation is very small in this process.

Remineralization. POM is assumed to be remineralized instantaneously below the euphotic zone. Horizontal advection of POM will be negligible, as the settling speed of POM is about 100m/day [*Suess et al.*, 1980], which is much faster than horizontal advection.

The vertical profiles of vertical fluxes of POM and calcite assumed in our model are shown in Figure 2. In each case, the vertical profile of POM flux is represented

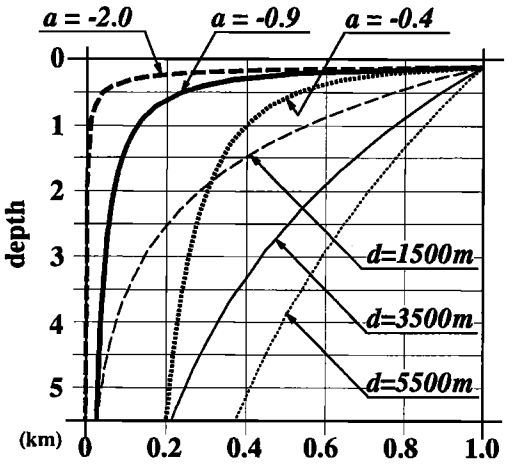

Figure 2. Vertical profiles of POC and calcite fluxes used in the B-GCM.

in the form of $(z/100\text{m})^a$. Case studies are performed for the three profiles : $a = -0.9$ (POM control profile), $a = -2.0$ (POM shallow profile), and $a = -0.4$ (POM deep profile). The control profile yields a vertical flux intermediate between particulate organic nitrate ($a = -0.988$) and POC ($a = -0.858$) fluxes obtained from the sediment traps [*Martin et al.*, 1987]. This profile is also similar to the profile of POC flux observed by *Suess et al.* [1980]. All POM which reaches the bottom is assumed to be remineralized.

Dissolution of POM under anoxic condition may be important for the distribution of tracers especially in the eastern equatorial Pacific and the Gulf of Guinea. The dissolution of POM in these regions is not due to oxygen utilization but it is due to denitrification. We consider the following treatment for POM dissolution under such a condition. The POM is always remineralized even in the anoxic or the euoxic layer. If dissolved oxygen concentration has a negative value during the time integration, the value is reset to zero to represent the effect of denitrification.

The calcite downward flux obtained by many sediment traps in the world ocean [*Tsunogai and Noriki*, 1991] suggests that calcite is hardly remineralized in the water column. On the other hand, analysis of the observed data by *Anderson and Sarmiento* [1994] suggests that a significant amount of $CaCO_3$ is remineralized at much shallower depths in the Indian and Pacific Ocean. Since the vertical profile of calcite is uncertain, we use a simple exponential form $\exp(-z/d)$, where d is an e-holding length scale of calcite flux, which is assumed to be 1500m(calcite shallow profile), 2500m, 3500m(calcite control profile), and 5500m(calcite deep profile), respectively. The vertical profile of calcite downward flux in our control case ($a = -0.09$, $R = 0.08$, and $d = 3500$m) is consistent with the observation by *Anderson and Sarmiento* [1994]. The remineralization ratio of calcite against total carbon is 15% at the depth of 1000m and

Table 1. Summary of Parameters and Results of Numerical Experiments in This Study

Experiment	Parameters				Results		
	a	d	R	r	CO_2	$\delta^{13}C$	EP
1	−0.9	3500	0.08	0.8	299	−6.60	9.9
2	−2.0	3500	0.02	2.5	302	−6.68	32.7
3	−0.4	3500	0.18	0.35	285	−6.50	4.2
4	−0.9	1500	0.14	0.8	301	−6.60	9.9
5	−0.9	5500	0.07	0.8	300	−6.61	9.9
6	−0.9	3500	0.08	1.0	289	−6.50	10.4
7	−0.9	3500	0.08	0.6	313	−6.75	8.9
8	−0.9	3500	0.08	0.3	352	−7.10	6.3
9	−2.0	3500	0.02	1.25	337	−7.01	22.3
10	−2.0	3500	0.02	0.75	364	−7.23	16.2
11	−0.4	3500	0.18	0.25	302	−6.67	3.7
12	−0.4	3500	0.18	0.125	342	−7.05	2.7
13	−0.9	5500	0.05	0.8	291	−6.59	9.9
14	−0.9	5500	0.08	0.8	305	−6.61	9.9
15	−0.9	3500	0.06	0.8	291	−6.59	9.9
16	−0.9	3500	0.07	0.8	295	−6.60	9.9
17	−0.9	3500	0.10	0.8	308	−6.62	9.9
18	−0.9	3500	0.16	0.8	335	−6.64	9.9
19	−0.9	2500	0.06	0.8	288	−6.59	9.9
20	−0.9	2500	0.08	0.8	294	−6.60	9.9
21	−0.9	2500	0.10	0.8	301	−6.61	9.9
22	−0.9	2500	0.11	0.8	305	−6.61	9.9
23	−0.9	2500	0.16	0.8	324	−6.63	9.9
24	−0.9	1500	0.08	0.8	287	−6.58	9.9
25	−0.9	1500	0.10	0.8	291	−6.59	9.9
26	−0.9	1500	0.16	0.8	306	−6.61	9.9
27	−0.9	1500	0.20	0.8	317	−6.62	9.9
28	no biota				483	−7.99	0

Here, a is an exponent appeared in the POC flux profile, d is e-holding length scale of calcite vertical flux (m), R is the rain ratio, r is the bioproduction efficiency (per year), CO_2 is the partial pressure of CO_2 in the atmosphere (micro atmospheres), $\delta^{13}C$ is ^{13}C in the atmosphere (per mil), and EP the export production(gigatons carbon per year). Experiment 1 is the control case.

45% at 4000m (*Anderson and Sarmiento* [1994] suggested 25% at 1000m and 50% at 4000m).

Initial condition and time integration. As an initial condition, the concentration of tracers is assumed to be homogeneous in the whole ocean. The concentration of phosphate is taken to be 2.1 μmol/kg, which corresponds to the average of observed values in the world ocean [*Levitus et al.*, 1993]. Similarly, the alkalinity is taken to be 2374 μeq/kg [*Takahashi et al.*, 1981]. The total CO_2 is assumed to be 2235 μmol/kg, which is slightly smaller than the preindustrial level (c.f., the present value of 2254 μmol/kg [*Takahashi et al.*, 1981]). The partial pressure of atmospheric CO_2 is assumed to be the preindustrial value of 280 μatm. The amount of ^{13}C is also assumed to be the preindustrial value, which is equivalent to $\delta^{13}C = -6.5‰$ in the atmosphere and $\delta^{13}C = 0.4‰$ in the ocean [*Kroopnick*, 1985]. Dissolved oxygen is assumed to be 200 μmol/kg.

We performed 28 case studies. Parameters and results in these cases are listed in Table 1. We obtain the distribution of tracers for each case, after carrying out the time integration for the 3000 years, which is considered to be long enough for achieving a steady state.

3. Biological Pump

Before showing the numerical results, we discuss the vertical transport of biogenic particulates such as POM and calcite. This is generally called the biological pump.

Strength of Biological Pump

An efficiency of vertical transport due to the biological pump is determined not only by the export production but also by the depth where biogenic particulates are effectively remineralized. In other words, this efficiency depends on the amount of particulate produced by biological activity and also on the effective length of vertical transport.

We define the strength of biological pump I, which is an index for the efficiency of vertical transport, as follows:

$$I = \int_{z_b}^{z_s} z \frac{dF(z)}{dz}\, dz, \tag{4}$$

where z represents depth ($z = z_s$ is the bottom of euphotic layer, and $z = z_b$ is the bottom of the ocean), and $F(z)$ is the downward vertical flux of settling biogenic particulate matter.

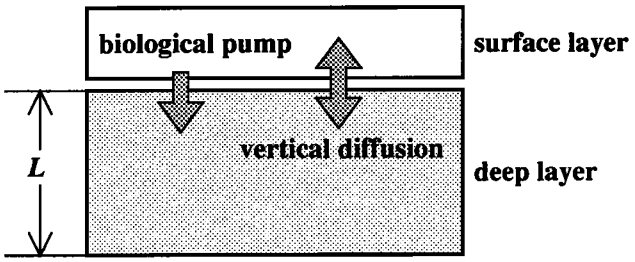

Figure 3. Two-box model for understanding the biological pump.

We also define the average remineralization depth L as the strength of biological pump divided by the export production, that is,

$$L \equiv \frac{I}{EP}, \tag{5}$$

where EP is the export production. In the control case ($a = -0.9$, $d = 3500$m), the average remineralization depths of POC and calcite are $L_{\mathrm{POC}} = 680$m and $L_{\mathrm{calcite}} = 2820$m, respectively.

Here we discuss the relation between the strength of biological pump and the difference in the concentration of tracers such as phosphate between the surface and the deep layer, by using a two-box model (Figure 3). We divide the ocean into two boxes: the surface and the deep layer. We can roughly consider that the biological pump affects the concentration of tracers in the deep layer shallower than the average remineralization depth L, but does not change the concentration in the layer deeper than L. Therefore, we take the length of the deep layer to be the average remineralization depth L.

The fluxes between the two boxes are assumed to be due to the biological pump and vertical diffusion. The equation of mass conservation of tracer in the deep layer is

$$L\frac{dC}{dt} = EP - \frac{k\Delta C}{L}, \tag{6}$$

where ΔC is the difference of concentrations of tracer between two boxes, and k represents the vertical diffusion coefficient. Then, in a steady state, we obtain the following relation,

$$I = EP \times L = k\Delta C. \tag{7}$$

The strength of biological pump is proportional to the difference of concentrations between the surface and the deep layer. This means that the difference in concentration depends not only on the export production but also on the depth where biogenic particulate matter is remineralized. Note that the export production must be large to keep the same difference, when the averaged remineralization depth is shallow. The large export production must be balanced by large vertical diffusion, as the biological pump with a shallow remineralization depth makes a steep vertical gradient of concentration. Although the effects of vertical advection and horizontal diffusion/advection are not considered in the above discussion, this expression will be appropriate for the real ocean, as discussed in section 5.

Rain Ratio

The ratio of the difference of total CO_2 concentrations between the surface and the deep layer ($= \Delta[TCO_2]$) to that of alkalinity ($= \Delta[\mathrm{Alk}]$) is 3~4. It is known that this ratio is accounted for by the two-box model with the rain ratio of 0.25 [e.g., *Broecker and Peng*, 1982]. The differences in both total CO_2 and alkalinity are determined by dissolutions of POC ($= \Delta C_{\mathrm{POC}}$) and calcite ($= \Delta C_{\mathrm{calcite}}$) in the deep water as follows:

$$\begin{aligned} \Delta[TCO_2] &= \Delta C_{\mathrm{POC}} + \Delta C_{\mathrm{calcite}} \\ \Delta[\mathrm{Alk}] &= -\frac{16}{106}\Delta C_{\mathrm{POC}} + 2\Delta C_{\mathrm{calcite}}, \end{aligned} \tag{8}$$

that is,

$$\frac{\Delta C_{\mathrm{calcite}}}{\Delta C_{\mathrm{POC}}} = \frac{16/106(\Delta[\mathrm{Alk}]/\Delta[TCO_2]) + 1}{2(\Delta[\mathrm{Alk}]/\Delta[TCO_2]) - 1} \simeq 0.25. \tag{9}$$

Figure 4 shows the widely used two-box model and ours. In the two-box model proposed in Figure 4a, the average remineralization depth of POC and that of calcite are implicitly assumed to be the same (i.e., $L_{\mathrm{POC}} = L_{\mathrm{calcite}}$). However, in the real ocean, L_{POC} is much shallower than L_{calcite}, and thus we must consider the difference of the average remineralization depths (Figure 4b). We therefore modify the rain ratio R as follows:

$$\begin{aligned} R &\equiv \frac{EP_{\mathrm{calcite}}}{EP_{\mathrm{POC}}} = \frac{I_{\mathrm{calcite}}}{I_{\mathrm{POC}}}\frac{L_{\mathrm{POC}}}{L_{\mathrm{calcite}}} \\ &= \frac{\Delta C_{\mathrm{calcite}}}{\Delta C_{\mathrm{POC}}}\frac{L_{\mathrm{POC}}}{L_{\mathrm{calcite}}} \simeq 0.25 \times \frac{L_{\mathrm{POC}}}{L_{\mathrm{calcite}}}. \end{aligned} \tag{10}$$

Only when the average remineralization depth of calcite is equal to that of POC, the rain ratio is 0.25. However, $L_{\mathrm{calcite}} = L_{\mathrm{POC}}$ is an unrealistic assumption, because L_{calcite} is at least two or three times deeper than L_{POC}. Therefore, the rain ratio R is < 0.12 at most. Since L_{POC} in the control case is estimated to be 680m and L_{calcite} is estimated to be 2820m, the rain ratio is expected to be about 0.06, which is much smaller than the value of 0.25 estimated by the widely used two-box model. *Bacastow and Maier-Reimer* [1990] used the rain ratio of 0.15. This is probably because their POC flux was assumed to be remineralized at the depths deeper than those estimated from the observed POC flux.

For application of this result to the real ocean, we must note the following two points. First, the two-box model is too simple to be directly applied to the real ocean. The effect of solubility pump which tends to underestimate the rain ratio is ignored in the discussion above. Also, the complexity of real ocean circulation

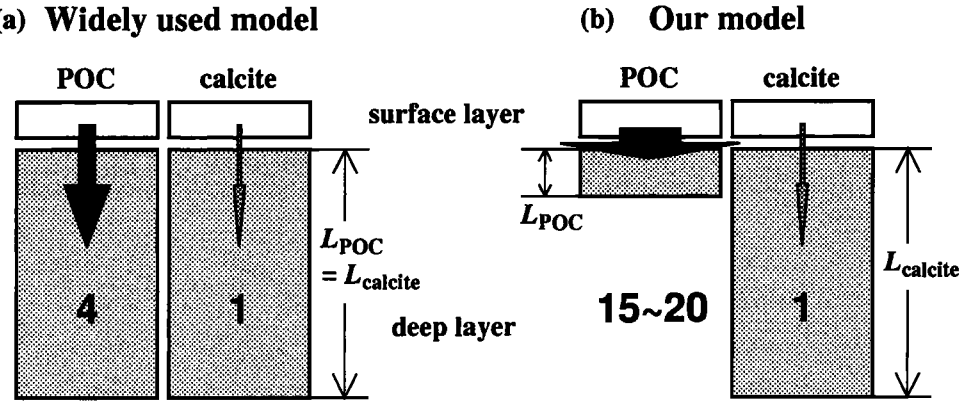

Figure 4. The difference between the widely used model and ours.

may increase uncertainty of the estimation of the rain ratio in the two-box model. However, the most reasonable estimate from our B-GCM in section 5 yields $R = 0.06 \sim 0.08$, which is slightly different from R estimated in the two-box model. Second, the sedimentation and the river input processes are not included in our model. At first glance, one might consider that, even when we take into account these processes, the total amount of tracers in the ocean is conserved in a steady state, as the river input rate is balanced with the sedimentation rate. However, since the production rate of calcite is balanced with its remineralization rate (which is included in our model) and its sedimentation rate (which is not included), the production rate of calcite obtained in our model should be underestimated. Thus we must include the contribution of calcite sedimentation to the rain ratio in order to apply our model to the real ocean. The sedimentation rate of calcite is estimated to be 0.2 Gt/yr for the world ocean [*Sundquist*, 1985]. With the export production of 9.9 Gt/yr estimated in our model, this is equivalent to the rain ratio of 0.02. This must be added to the value of 0.06 to approximately 0.08 which is obtained from our B-GCM.

Thus we find that the rain ratio should be 0.08 to approximately 0.10 in the real ocean. This estimate is consistent with the observations [*Tsunogai and Noriki*, 1991; *Takahashi et al.*, 1990]. From the sediment trap data [*Tsunogai and Noriki*, 1991], we estimate the ratio of calcite flux against POC flux at the depth of 1km to be 0.51 as the weighted mean by using calcite flux. This is equivalent to the rain ratio of 0.07 defined at the bottom of the euphotic layer. *Takahashi et al.* [1990] reported from the Joint Global Ocean Flux Study (JGOFS) site at 47°N-20°W that the ratio of production rate of POC against that of calcite (i.e., $1/R$) is 9 ± 2, which is equivalent to the rain ratio of 0.11 ± 0.03. All these observational estimates roughly coincide with our estimate of 0.08 to approximately 0.10, which is obviously much smaller than the value (= 0.25) estimated by the widely used two-box model.

4. Results

In this section, we describe the results of the control case (experiment 1) of our biogeochemical general circulation model. Figures 5 through 7 show that meridional mass transport and distributions of temperature and salinity in the Atlantic and the Pacific meridional sections.

Physical Fields

Stream function of meridional mass transport in the Atlantic and the Pacific is shown in Figure 5. In the Atlantic, the maximum transport of NADW is 24Sv ($= 24 \times 10^6 m^3/s$), and the outflow to the Southern Ocean is 17Sv. As was stated in section 2, we use the reference sea surface temperature lower than the annual condition for the northern North Atlantic so that the transport of NADW may be comparable with the observation [e.g., *Rintoul*, 1991]. The maximum transport of the Antarctic Bottom Water (AABW) is 4Sv. In the Pacific, the inflow below the depth of 2km is 6Sv. This is considered to be slightly smaller than the real ocean, as the meridional contrast of $\Delta^{14}C$ in the deep water is stronger than the GEOSECS observation, which will be discussed later. The Ekman circulation, a meridional circulation driven by wind stress, is limited to the layer above the depth of 500m.

Distributions of temperature along GEOSECS sections in the western Atlantic and the western Pacific are shown in Figures 6. The isotherm of 10°C lies at about 500m depth in the Atlantic and the Pacific, and the isotherm of 5°C lies at about 1000m in the Pacific. The thermocline depth in the Atlantic and the Pacific (see Figure 15) is reproduced better than that in the previous studies [e.g., *Toggweiler et al.*, 1989], although it is deeper than the observed, which is due to the small value for the vertical diffusion coefficient adopted in our model.

The temperature of NADW is about 2K warmer than the observed because the cold overflow water across the

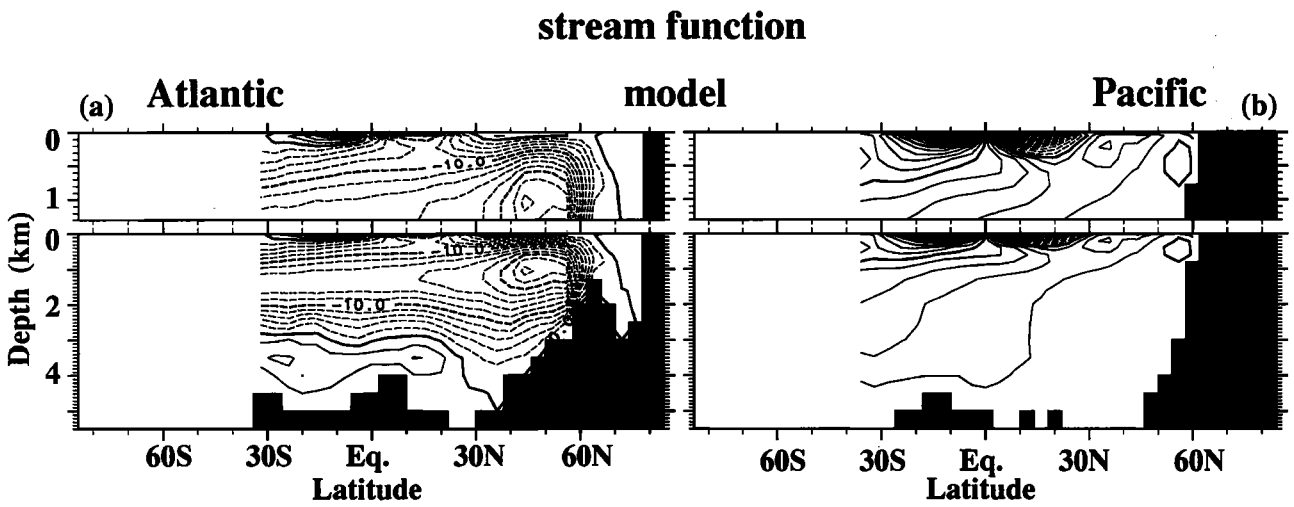

Figure 5. Stream function of meridional mass transport for (a) the Atlantic and (b) the Pacific. Contour interval is 2Sv (1Sv=$10^6 m^3/s$).

straight of Iceland-Scotland is not reproduced in our model. The temperature of the Pacific bottom water is about 1°C, which is consistent with the observation.

Distributions of salinity along the GEOSECS sections are shown in Figure 7. In the Atlantic, the salinity minimum water is well reproduced due to the small values for the vertical and horizontal diffusion coefficients. On the other hands, AABW is far less saline than the observed. This is because the reference value of sea surface salinity was taken as the annual mean condition

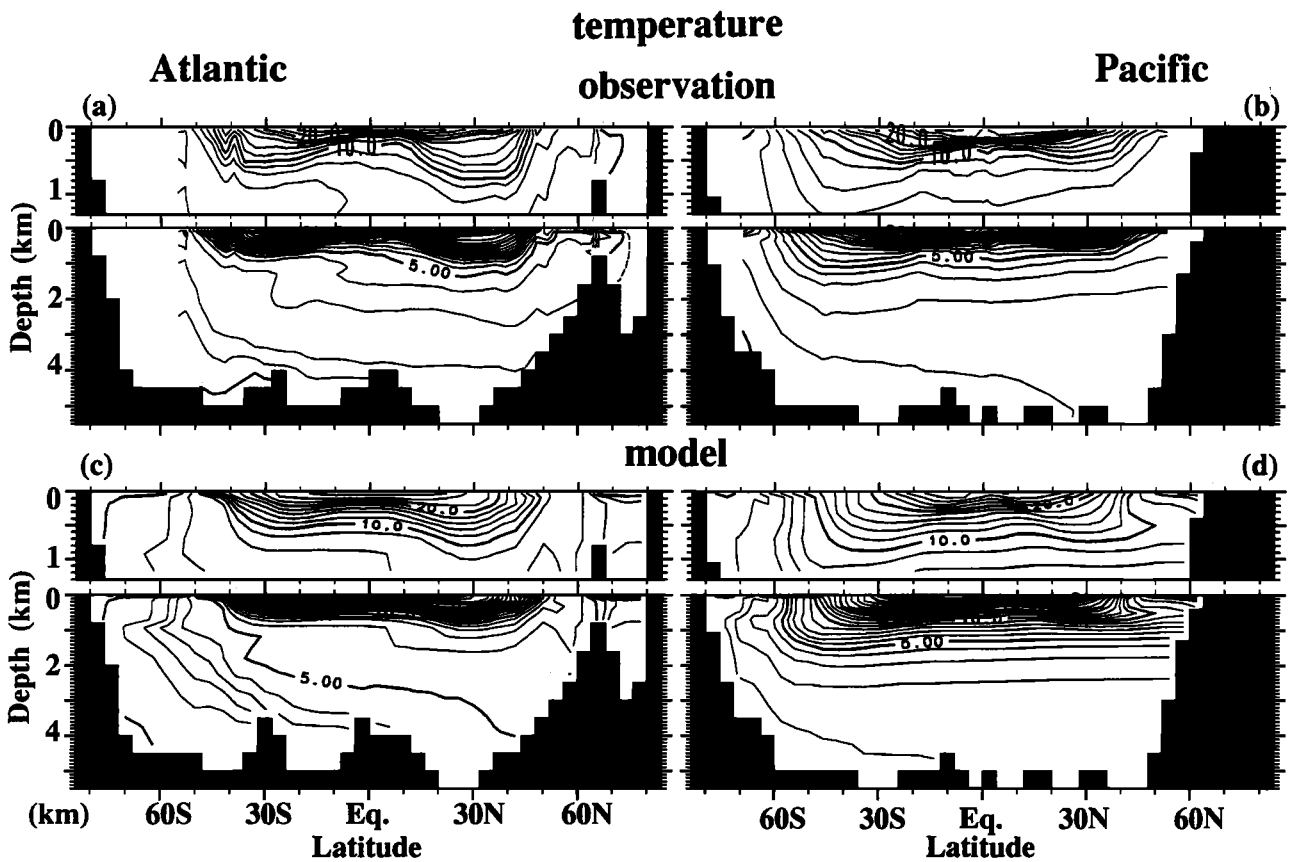

Figure 6. Temperature distributions along the Geochemical Ocean Sections Study (GEOSECS) sections in the western Atlantic (left-hand side) and the western Pacific (right-hand side): (a,b) observation and (c,d) model results. Contour interval is 1K and 2K (> 1km).

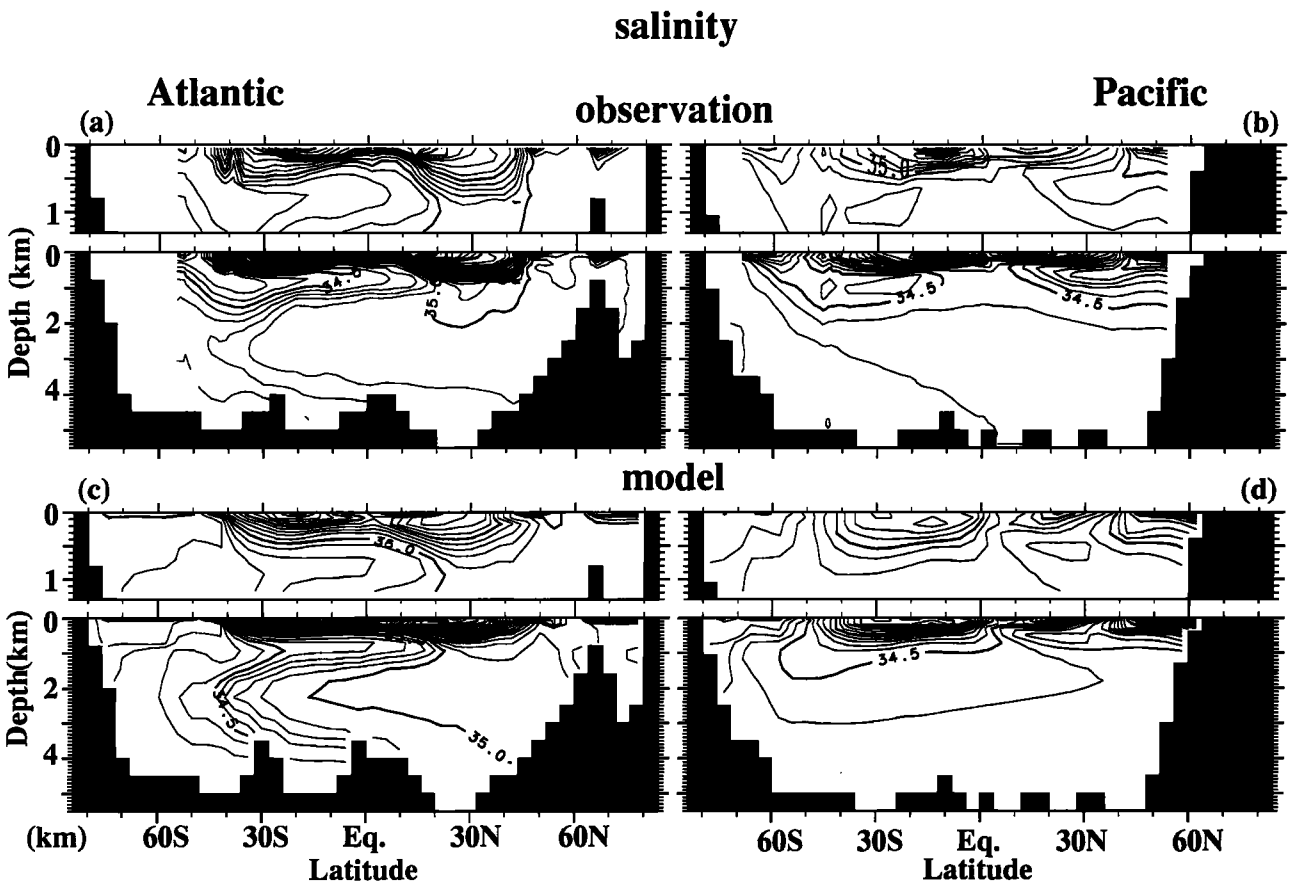

Figure 7. Salinity, as in Figure 6. Contour interval is 0.1psu. and 0.2psu (> 1km)

for the Ross and Weddell Seas (the reference sea surface salinity higher than the observed is often used to take into account the effect of the brine rejection by sea ice formation in midwinter [e.g., *England*, 1993]). Since AABW is less saline, the salinity of the Pacific deep water becomes lower than the observed, and Antarctic Intermediate Water (AAIW) does not appear in the Pacific. The depth and strength of the North Pacific Intermediate Water (NPIW) is compared with the observation.

Although some features such as the warmer NADW and the less saline AABW require further improvement of the model, the flow fields and the distributions of temperature and salinity seem to be well reproduced on the global scale. The maximum value of meridional heat transport is 1.4 PW (= 10^{15}W) for the northern hemisphere and 1.6 PW for the southern hemisphere, which are comparable with the observations. Figures 8 through 13 show the distributions of the various chemical tracers along the GEOSECS sections in the western Atlantic and the western Pacific.

Distribution of $\Delta^{14}C$

The distributions of $\Delta^{14}C$ along the GEOSECS sections are shown in Figure 8. Here $\Delta^{14}C$ is a passive tracer and its distribution is determined only by the flow fields and decay time, although the gas exchange between the atmosphere and the ocean has some influence. Therefore, the distribution of $\Delta^{14}C$ is useful for understanding the abyssal circulation.

The values of $\Delta^{14}C$ of the deep water in the North Atlantic and the North Pacific are $-60‰$ and $-250‰$, respectively, which are well compared with the observation [*Stuiver and Ostlund*, 1980; *Ostlund and Stuiver*, 1980]. Since the flow is slightly stronger in the Atlantic, the value of $\Delta^{14}C$ in the Southern Ocean becomes younger than the observed. The value of the model result above the depth of 750m is lower than the observed because the bomb $\Delta^{14}C$ is not taken into account in our model.

Distributions of Phosphate and Dissolved Oxygen

Figure 9 shows the distributions of phosphate along the GEOSECS sections. The phosphate maximum is found at about 1200m depth in the Pacific and at about 800m depth in the Atlantic, which is well compared with the observation. In the Atlantic, this maximum seems to spread as a tongue from the Southern Ocean. The maximum value of 3.4 μmol/kg is found in the

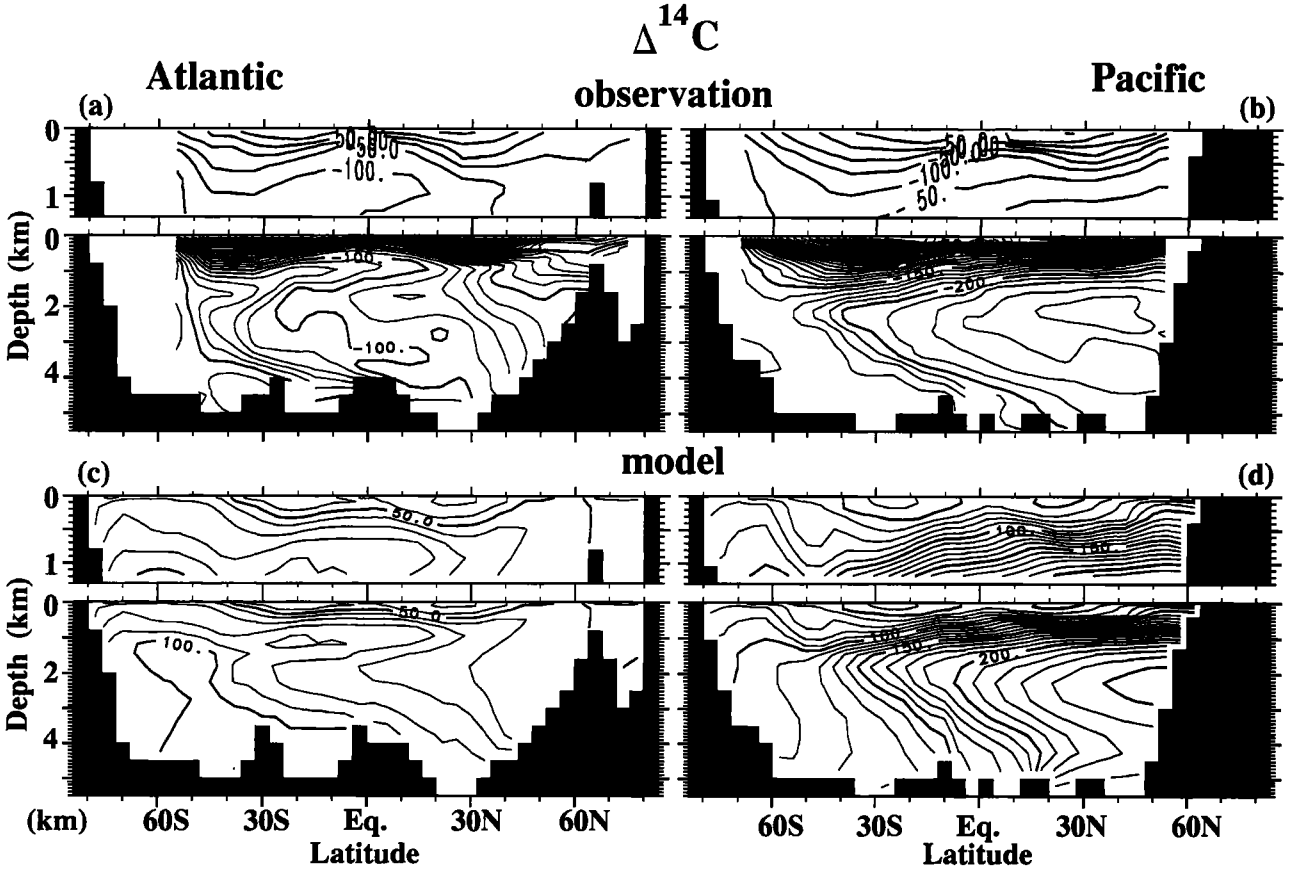

Figure 8. $\Delta^{14}C$, as in Figure 6. Contour interval is 10‰ and 50‰(>1km in the observation). Note that the nuclear bomb ^{14}C is not taken into account in our model.

northern part of the North Pacific. This is comparable with the observed value of >3.2 μmol/kg [*Levitus et al.*, 1993]. There are regions of high phosphate concentration above the thermocline depth of about 500m, which corresponds to the area of high export production. This is explained by the mechanism of the nutrient trapping [*Najjar et al.*, 1992]. Below the thermocline depth, phosphate concentration increases gradually from the North Atlantic to the North Pacific with increase in age of the water (which is estimated from $\Delta^{14}C$ value).

The dissolved oxygen minimum exists in the Atlantic and the Pacific (see Figure 10). The depth of the dissolved oxygen minimum is shallower than that of the phosphate maximum, as the deep water formed at high latitudes is colder and richer in oxygen than a normal surface water is. The minimum value of about 10.0 μmol/kg is found in the northern part of the Northern Pacific, which is comparable with the observed value [*Levitus*, 1982].

Distributions of Total Carbon Dioxide and Alkalinity

Figure 11 shows the distributions of total CO_2 along the GEOSECS sections in the western Atlantic and the western Pacific. The total CO_2 maximum is found at about 2km depth in the Pacific and in the layer of the phosphate maximum in the Atlantic. The maximum value in the North Pacific is about 2400 μmol/kg, which is well compared with the GEOSECS observed value [*Craig et al.*, 1981].

The distributions of alkalinity along the GEOSECS sections are shown in Figure 12. The alkalinity maximum is seen at about 2 to approximately 3km depth in the Pacific. The distribution of alkalinity is mainly determined by the vertical transport of calcite. In general, calcite is effectively dissolved in the layer deeper than POC is. The alkalinity maximum appears in the layer much deeper than the phosphate maximum. Horizontal contrast of alkalinity between the North Atlantic and the North Pacific is comparable with its vertical contrast between the surface and the deep water. The reason will be discussed in the next section.

Distribution of $\delta^{13}C$

The distributions of $\delta^{13}C$ along the GEOSECS sections are shown in Figure 13. The $\delta^{13}C$ minimum values in the Atlantic and the Pacific are 0.7‰ and -0.6‰ , respectively, which are well compared with the GEOSECS observation [*Kroopnick*, 1985]. The distribution of $\delta^{13}C$

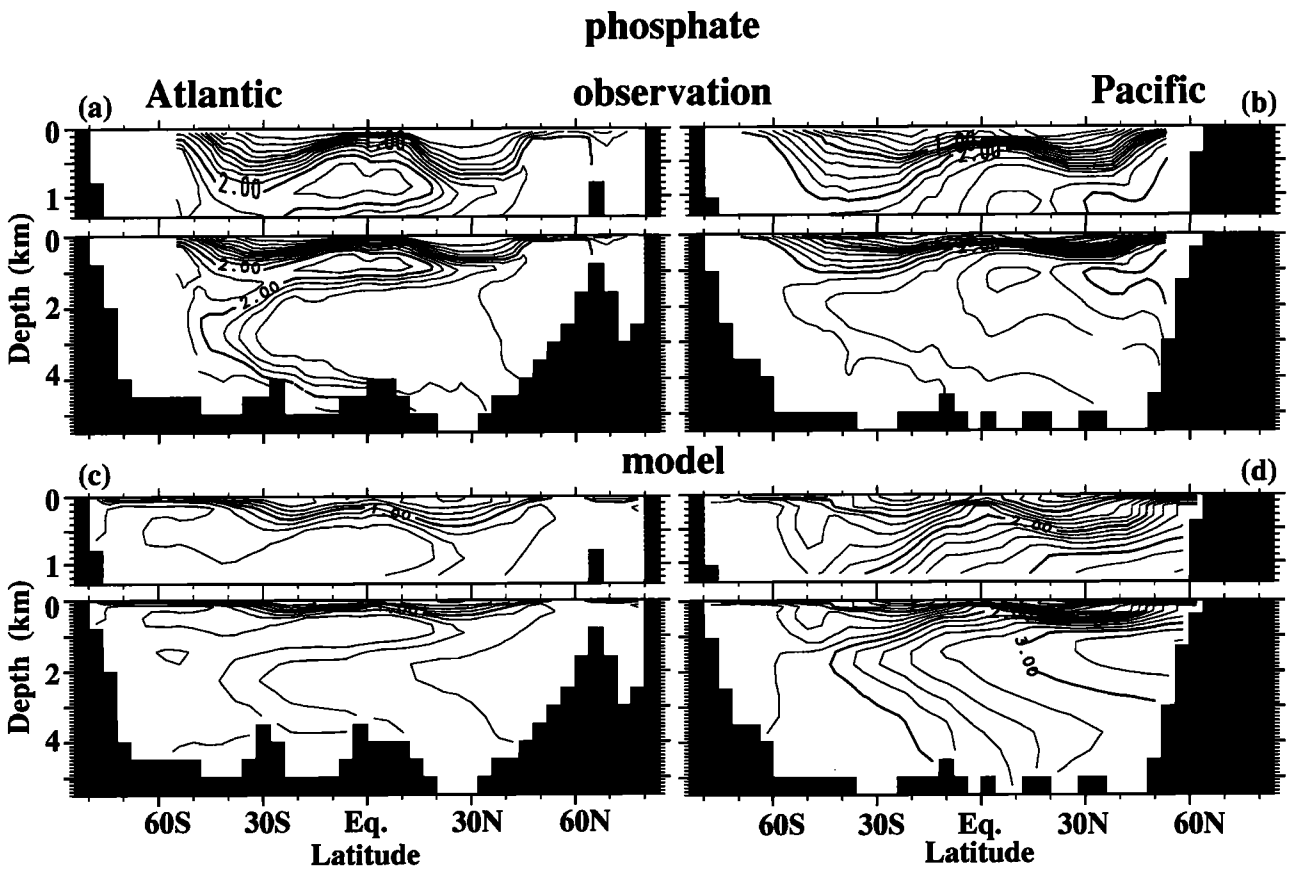

Figure 9. Phosphate, as in Figure 6. Contour interval is 0.2μmol/kg.

is roughly considered to be the mirror image of the distribution of phosphate as these distributions are determined mainly by the vertical transport of POC although there is an effect of gas exchange on $\delta^{13}C$. The atmospheric $\delta^{13}C$ becomes $-6.60‰$, which is consistent to the preindustrial value [*Kroopnick*, 1985].

Horizontal Distribution of ΔpCO_2

The partial pressure of CO_2 in the atmosphere is 299μatm. Figure 14 shows the distribution of ΔpCO_2 which represents the difference in partial pressure of CO_2 between the atmosphere and the ocean. Figures 14a and 14b are for the observation by *Tans et al.* [1990], and Figure 14c for our results. Since the simulation is performed under the annual mean condition and that for the preindustrial state, direct comparison of ΔpCO_2 between the model results and the observation may be difficult. The following rough features in the observed ΔpCO_2 distribution is simulated by our model. In the equatorial Pacific, pCO_2 in the ocean is >100μatm higher than that in the atmosphere due to the upwelling of the deep water with high pCO_2. In the subtropical region, the oceanic pCO_2 is lower than the atmospheric pCO_2 by the effect of biological pump. In the northern North Atlantic, pCO_2 of the seawater is much lower than that of the atmosphere, as NADW exports the total CO_2 out of this region in association with the formation of deep water [*Broecker and Peng*, 1992]. The high and the low pCO_2 regions appear to spread, somewhat randomly, over the other area at high latitudes. In the area of high pCO_2, the CO_2-rich water is brought up from the subsurface layer by convection.

5. Discussion

To extend an ocean general circulation model to include biogeochemical processes, we must introduce many biogeochemical parameters. Although these processes appear to be complicated, distributions of biogeochemical tracers are determined mainly by the following four parameters: the exponent of vertical profile of POM flux a, the bioproduction efficiency r, the e-holding length scale of calcite flux d, and the rain ratio R. In this section we will discuss about these parameters.

Case Studies for Various Vertical Profiles of POM Flux

We study an effect of change in the prescribed profile of POM flux. We calculate the following 10 cases: $a = -0.9$ (POM control profile; experiment 1, 6 through

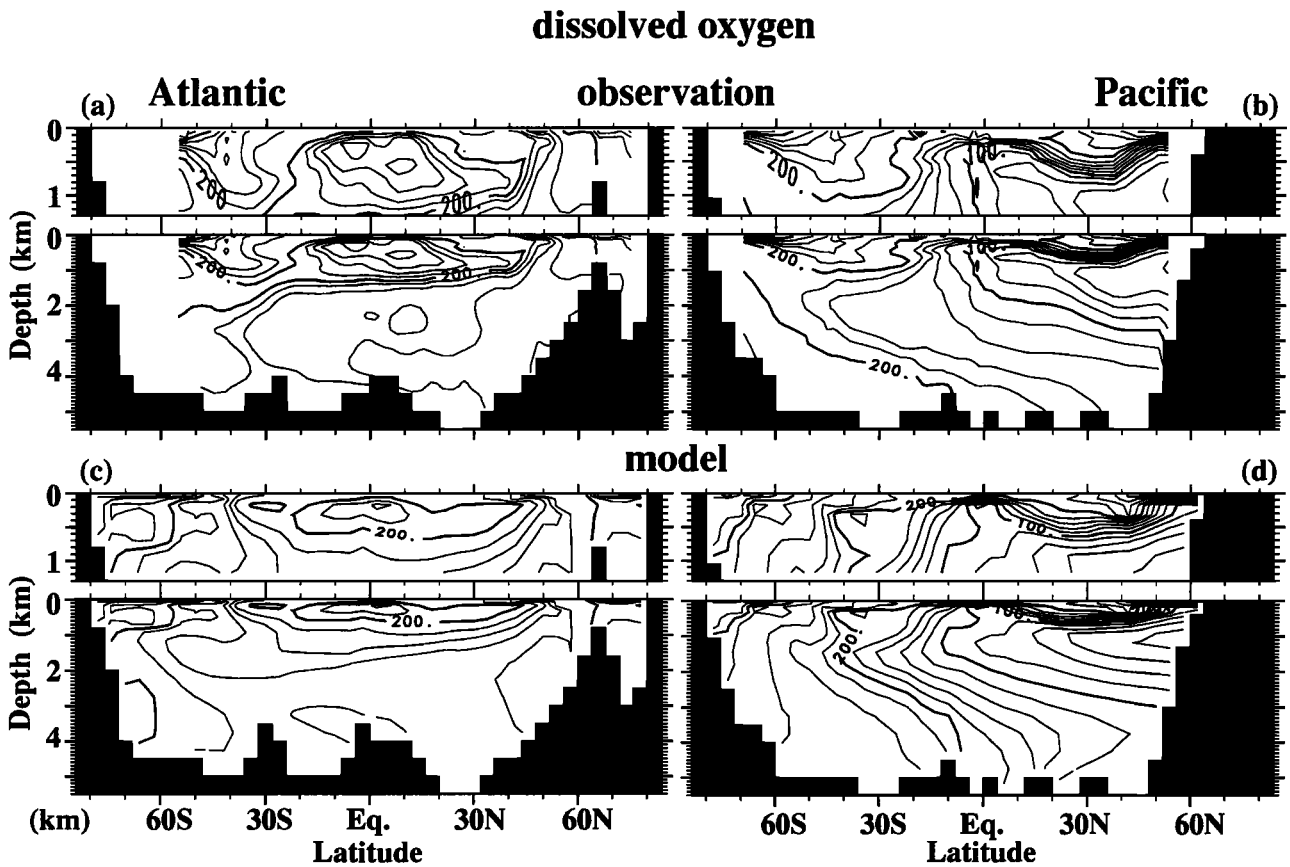

Figure 10. Dissolved oxygen, as in Figure 6. Contour interval is 20μmol/kg.

8), $a = -2.0$ (POM shallow profile; experiment 2, 9, 10), and $a = -0.4$ (POM deep profile; experiment 3, 11, 12). The phosphate distribution depends only on two parameters, the exponent of POC flux a and the bioproduction efficiency r. In this subsection we will discuss the dependency of phosphate distribution on two parameters. Values of parameters for each case are shown in the Table 1.

Vertical phosphate distribution. We discuss the vertical distribution of phosphate in the three cases, experiment 1 (POM control profile), experiment 2 (POM shallow profile), and experiment 3 (POM deep profile). Figure 15 shows the horizontally averaged vertical distributions of temperature and phosphate at the GEOSECS locations in the world ocean. With given a, the estimate of r in the three cases of Figure 15b is obtained by fitting the observed difference of phosphate concentration between the surface and the deep layer, because this difference is roughly determined by a and r as was discussed in section 3 (see equation (7)). However, vertical distributions of phosphate concentration in these cases are not same. The depth of phosphate maximum is 700m (POM shallow profile), 1300m(POM control profile), and 5500m(POM deep profile), respectively. As clearly seen in Figure 15b, the vertical profile of phosphate concentration for the POM control profile is well compared with the observation. The gradient of phosphate concentration at the thermocline depth for the POM control profile is sightly smaller than the observed, as the temperature at this depth in our model is warmer than the observed. Thus, the optimal estimates of a and r can be determined by comparing the vertical phosphate distribution in our model with the observation.

Horizontal phosphate distribution. We discuss the horizontal distribution of phosphate in the three cases, experiment 2 (POM shallow profile), experiment 1 (POM control profile), and experiment 3 (POM deep profile). Figure 16 shows the distributions of phosphate along the GEOSECS western Atlantic and western Pacific sections. For the POM shallow profile, the nutrient trapping occurs excessively above the depth of 500m, as the very high concentration is found at the depth of 200m in the equatorial Pacific. Below the depth of 1000m, on the other hand, the horizontal contrast of phosphate concentration is much weaker than the observed. In experiment 3 (POM deep profile), there is no phosphate maximum layer in the North Pacific.

The phosphate concentration in the North Atlantic decreases with an increase of the average remineraliza-

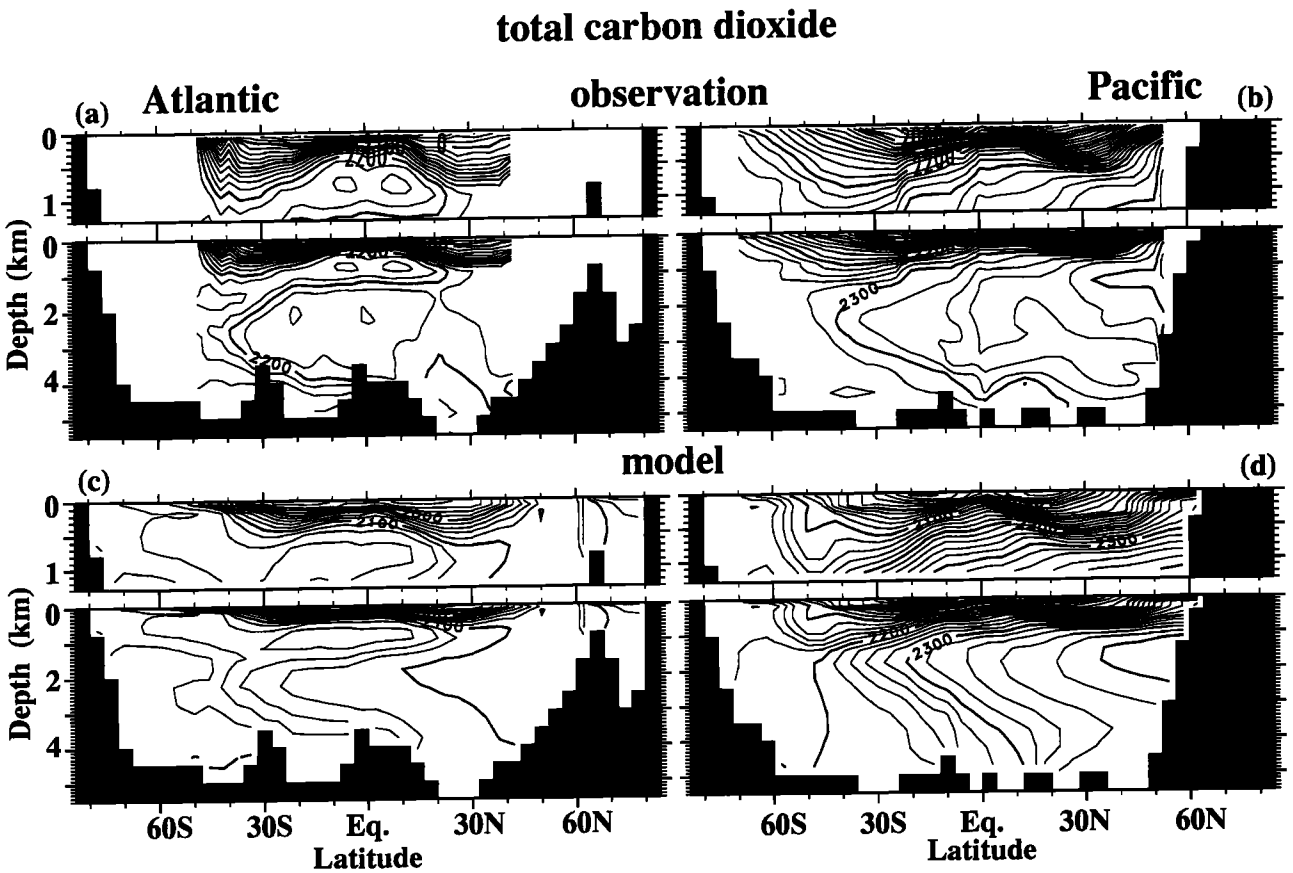

Figure 11. Total CO_2, as in Figure 6. Concentration of total CO_2 is normalized by salinity of 35psu. Contour interval is 20μmol/kg. Note that the anthropogenic carbon is not taken into account in our model.

tion depth ($a = -2.0 \rightarrow -0.9 \rightarrow -0.4$). In the North Pacific, on the other hand, it increases with an increase of the average remineralization depth. Horizontal contrast of phosphate in the deep water also depends on the vertical profile of POM flux. The horizontal contrast increases with an increase of the average remineralization depth. The reason is as follows: although the export production for the POM deep profile is smaller than that for the POM control profile, the amount of remineralization of POM in the deep water is larger. Besides, the horizontal advective-diffusive flux is dominant in the deep layer. Then, the deep water becomes rich in phosphate due to the remineralization of POM in the course of advection from the North Atlantic to the North Pacific. Therefore the horizontal contrast of phosphate concentration increases with an increase of the remineralization depth. The horizontal contrast of phosphate for the POM control profile (the observed profile of POM flux by sediment trap is $a = -0.9$) provides the most appropriate result among the three profiles. Thus, the optimal estimates of a and r can be also determined by comparing the horizontal phosphate distributions in our model with the observation.

The ratio of the horizontal against vertical contrast of phosphate concentration increases with an increase of the remineralization depth of POM downward flux. For example, when a is large (POM shallow profile), the horizontal contrast is smaller than the vertical. When it is small (POM deep profile), the horizontal contrast is on the same order of magnitude as the vertical. The results of case studies for using various r (experiment 1 and experiment 6 through 8) show that both the vertical and the horizontal contrasts become stronger with an increase of r while roughly keeping a constant vertical against horizontal contrast ratio. Using the above features of a and r, we can determine the optimal set of these values as was discussed above. The optimal value of a determined from the phosphate distribution coincides with the value obtained from many sediment trap observations [e.g., *Martin et al.*, 1987; *Suess et al.*, 1980]. This means that the observed value of a can reasonably explain the observed phosphate distribution.

Export production. Figure 17 shows a plot of the export production against the concentration of atmospheric CO_2 in each case. In the control case, the export production is estimated to be 9.9GtC/yr, correspond-

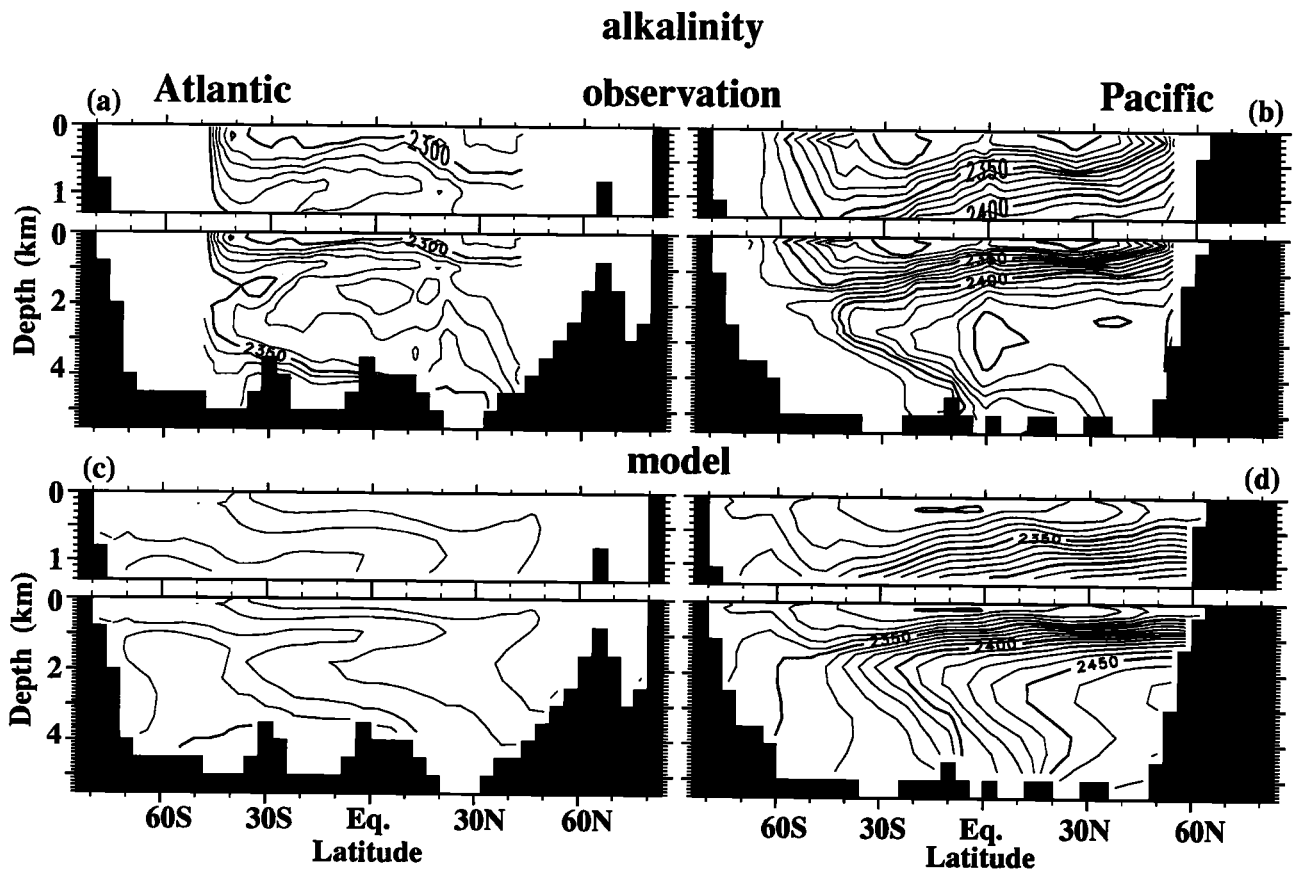

Figure 12. Alkalinity, as in Figure 6. Concentration of alkalinity is normalized by salinity of 35psu. Contour interval is 20μeq/kg.

ing to the atmospheric CO_2 level of 299μatm. Since the atmospheric CO_2 reflects the concentration of total CO_2 in the surface water, the atmospheric CO_2 level also represents the global average concentration of total CO_2 in the surface water. With fixed atmospheric CO_2 level at 280 to approximately 300μatm (shaded area in Figure 17), the export production decreases with an increase of the average remineralization depth. As was discussed by using the two-box model in section 3, the difference in total CO_2 concentration between the surface and the deep layer depends on both the export production and the remineralization depth. Thus, equation (7) roughly holds also on the B-GCM. The export production for the POM shallow profile rapidly increases with a decrease of the atmospheric CO_2 level, because the phosphate concentration under the high-productivity area increases due to the nutrient trapping.

The value of the export production is automatically determined from the optimal estimates of a and r. The export production consistent with the observed distribution of phosphate is estimated to be about 10GtC/yr (when we include DOC in our model, it is estimated to be about 9GtC/yr [*Yamanaka*, 1995]). This value is within the observed estimates which range from 3.4 to approximately 7.4GtC/yr [*Eppley*, 1989] to 20GtC/yr [*Packard et al.*, 1988].

Case Studies for Various Vertical Profiles of Calcite Flux

Next, we study an effect of change in the prescribed profile of calcite flux. We calculate the following 18 cases: d = 1500m (calcite shallow profile; experiment 4, 24 through 27), d = 2500m (experiment 19 through 23), d = 3500m (calcite control profile; experiment 1, 15 through 18), and d = 5500m (calcite deep profile; experiment 3, 13, 14).

Since the optimal estimates of a and r are determined by comparing the phosphate distribution in our model with the observation in the previous subsection, distributions of the other chemical tracers except alkalinity are automatically determined in our model. The alkalinity distribution depends only on two parameters, the e-holding length scale of calcite flux d and the rain ratio R, with fixed a and r. In this subsection, we will discuss the dependency of alkalinity distribution on the two parameters. Values of parameters for each case are shown in the Table 1.

Vertical alkalinity distribution in the world ocean. We discuss the vertical distribution of alkalinity in the three cases: experiment 4 (calcite shallow profile), experiment 1 (calcite control profile), and experiment 5 (calcite deep profile). Figure 18a shows the

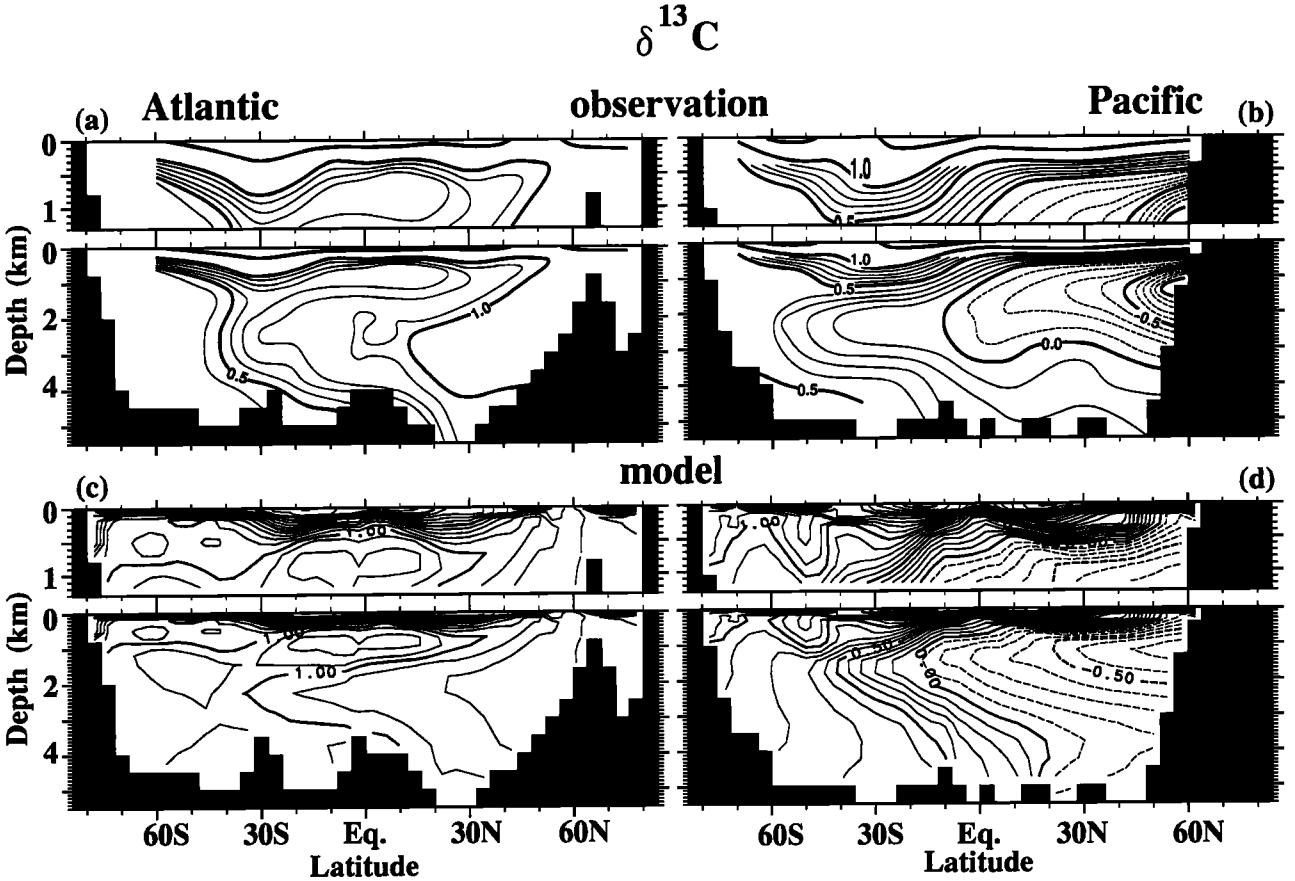

Figure 13. $\delta^{13}C$, as in Figure 6. Observation is after Kroopnick [1985]. Contour interval is 0.1‰.

horizontally averaged vertical distributions of alkalinity at the GEOSECS locations in the world ocean. With given d, the estimate of R in the three cases of Figure 18a is obtained by fitting the observed difference of alkalinity between the surface and the deep layer because this difference is roughly determined by d and R. However, vertical profiles of alkalinity in the three cases are not same. The alkalinity maximum in experiment 4 is found at the depth of 1500m. The value of alkalinity in experiment 5 monotonously increases with increasing depth.

The vertical profiles of alkalinity for the calcite control profile provide the most appropriate results among the three profiles. As clearly seen in Figure 18a, the alkalinity for the calcite shallow profile is distributed at much shallower depths than the observation. Thus the rough optimal estimates of d and R can be determined by comparing the vertical alkalinity distribution in our model with the observation.

Vertical alkalinity distributions in the Atlantic and the Pacific. We discuss the horizontal distribution of alkalinity in the three cases, experiment 4 (calcite shallow profile), experiment 1 (calcite control profile), and experiment 5 (calcite deep profile). Figure 18b shows the horizontally averaged vertical distributions of alkalinity at the GEOSECS locations in the Atlantic and the Pacific.

For the calcite shallow profile, the remarkable alkalinity maximum in the Pacific is found at the depth of 1500m. The value of alkalinity below the depth of 2200m in the Pacific is much less than the observed. The value of the shallow maximum at the depth of 1000m in the Atlantic is the same as the deep maximum at the depth of 4000m. For the calcite deep profile, the value of alkalinity in the Pacific monotonously increases with increasing depth. For the calcite control profile, the alkalinity maximum in the Pacific is found at the depth of 2250m, which is slightly shallower than the observed. The vertical distributions of alkalinity both in the Pacific and the Atlantic for the calcite control profile are best compared with the observation among the three profiles. The horizontal contrast of alkalinity between the Atlantic and the Pacific increases with an increase of d or with an increase of R. When the horizontal contrast is kept constant, R decreases with an increase of d. Therefore, the estimate of R for the calcite deep profile is smaller than that for the calcite shallow profile.

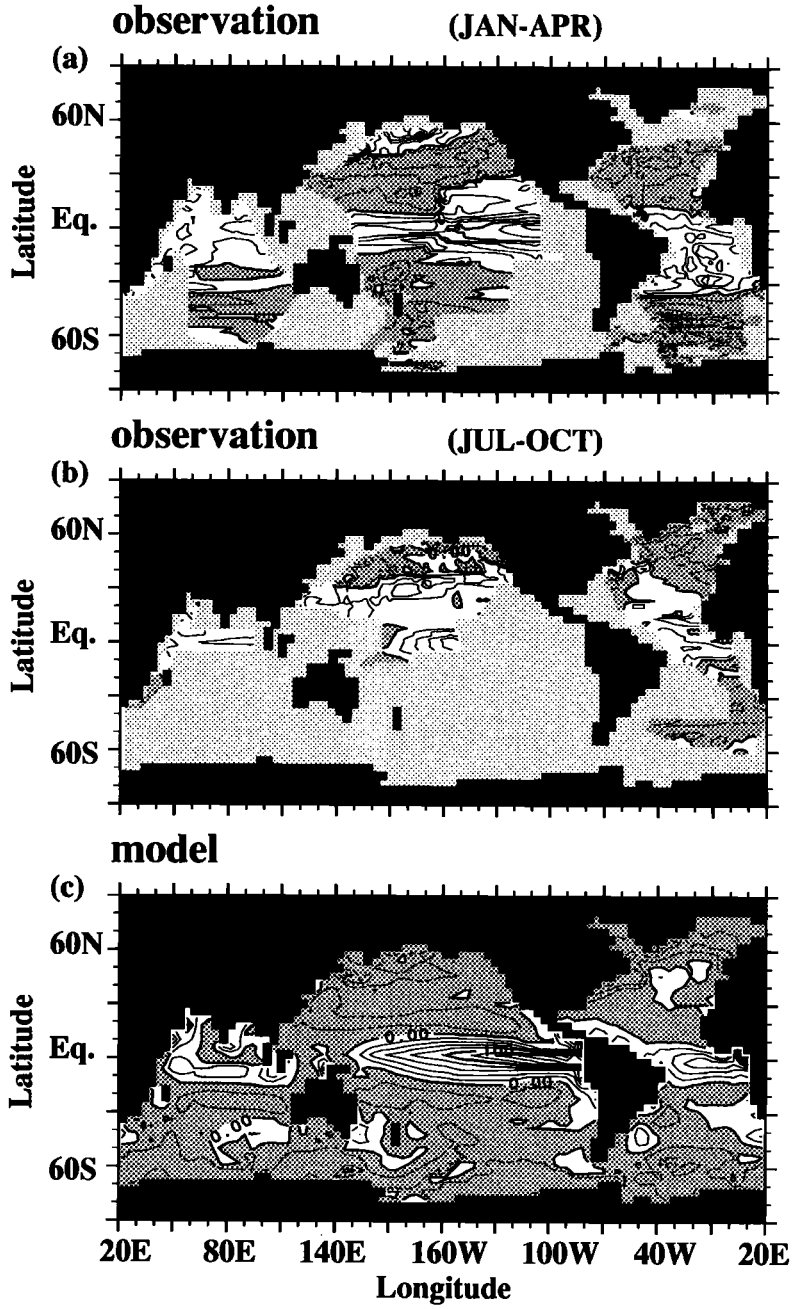

Figure 14. Horizontal distribution of ΔpCO_2 from (a) observation (JAN-APR), (b) observation (JUN-OCT), and (c) model result. Observations are after *Tans et al.*[1990]. Contour interval is 20μatm. Light shaded area represents the region without observation. Dark shaded area represents the region where the oceanic pCO_2 is lower than the atmospheric pCO_2.

Thus the optimal estimate of d and R can also be determined by comparing the vertical alkalinity distribution in both the Pacific and the Atlantic in our model with the observation.

Rain ratio. Figure 19 shows horizontally averaged vertical contrast of alkalinity between the surface and the deep waters (= Δ[Alk]) at the GEOSECS locations in the world ocean for each case. As clearly seen, this contrast increases with an increase of the rain ratio R or with an increase of the e-holding length scale d. When the vertical contrast is kept constant, R increases with an decrease of d, because the vertical contrast is mainly determined by d (which determines L_{POC}) and R (which determines production of alkalinity) as was discussed in section 3 (see equation (7)). Since the observed Δ[Alk] is about 70μmol/kg and the optimal estimate of d is about 3500m as was discussed above, the

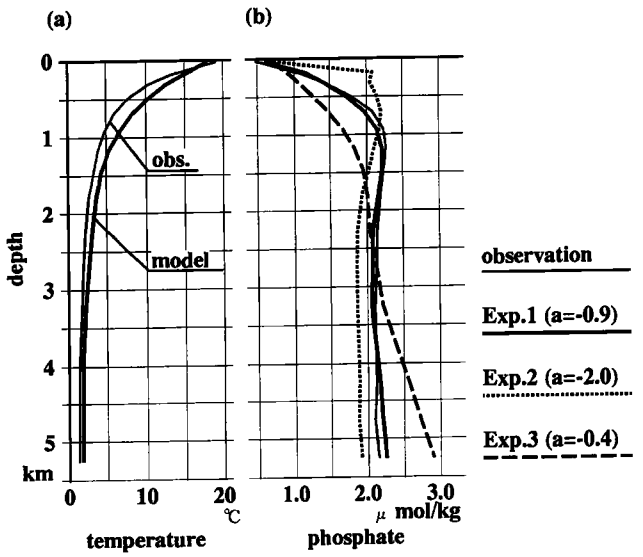

shaded area in Figure 19 represents the best fit to the observed alkalinity distribution. Therefore, the optimal estimate of rain ratio R is 0.06 to approximately 0.08.

Figure 20 shows a plot of alkalinity against total CO_2 in the surface and the deep water along the GEOSECS locations in the world ocean. This figure is usually used to illustrate the relation between the rain ratio and the distributions of alkalinity and total CO_2 [*Broecker and Peng*, 1982]. The contrast of alkalinity between the sur-

Figure 15. Horizontally averaged vertical profiles of (a) temperature and (b) phosphate at the GEOSECS locations in the world ocean. Thick solid lines, thick dotted lines, thick dashed lines are for the results in experiment 1 (POM control profile), experiment 2 (POM shallow profile), and experiment 3 (POM deep profile), respectively. Thin solid lines are for the GEOSECS observations.

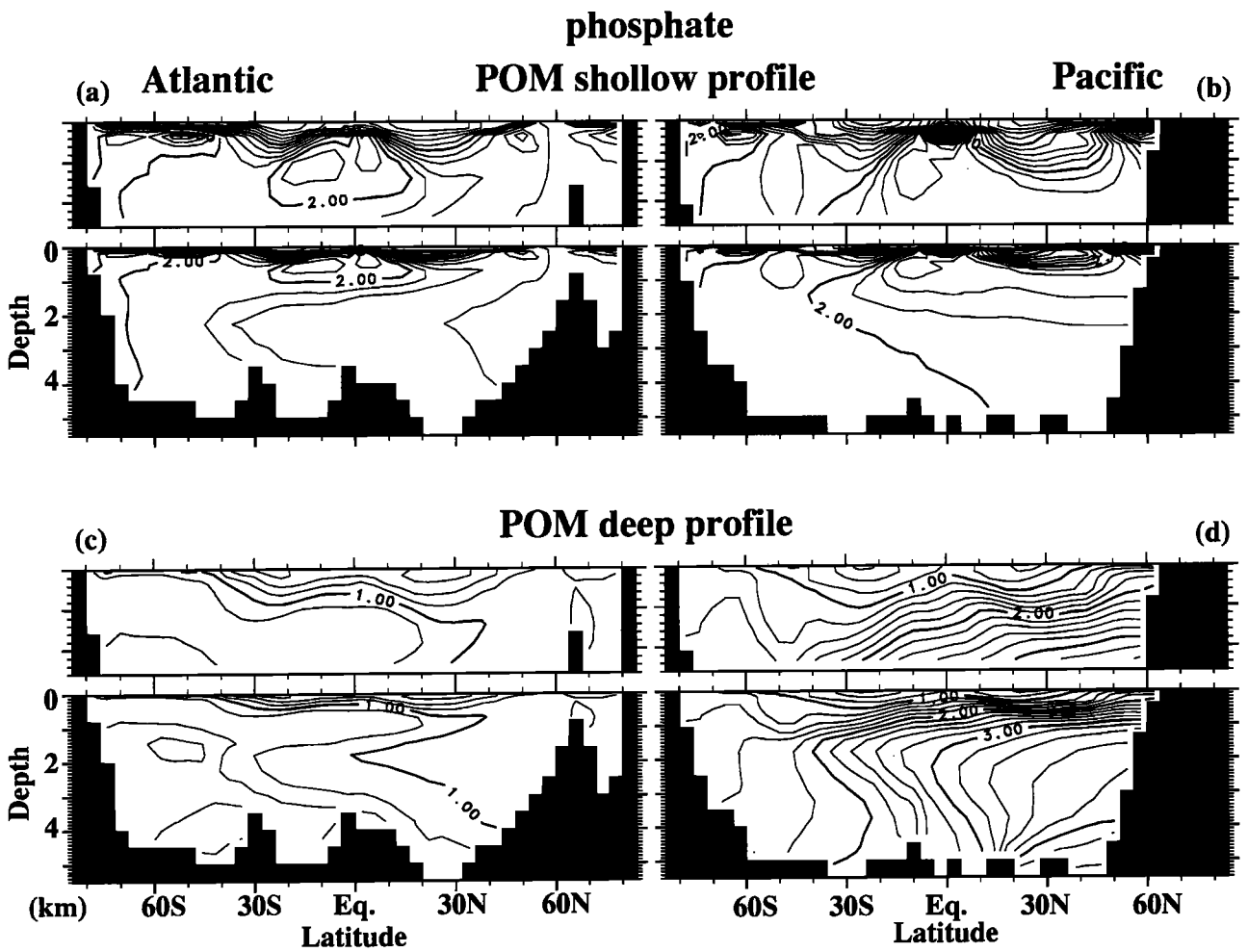

Figure 16. Meridional sections of phosphate along the GEOSECS western Atlantic (left-hand side) and the GEOSECS western Pacific (right-hand side): (a,b) the POM shallow profile (experiment 2) and (c,d) the POM deep profile (experiment 3). Contour interval is 0.2μmol/kg.

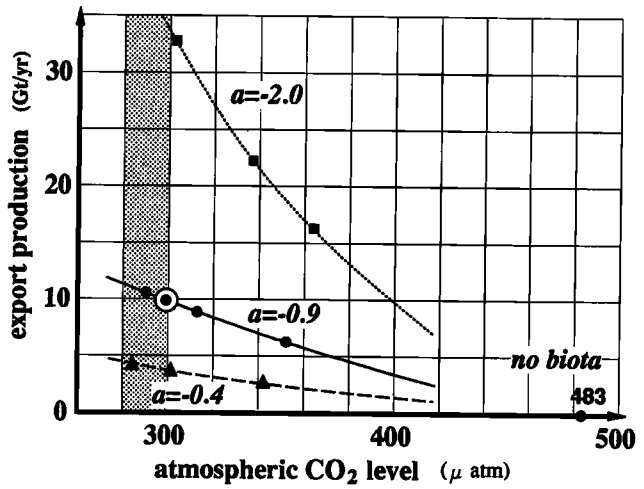

Figure 17. Plot of export production against the atmospheric CO_2. Circle represents the POM control profile ($a = -0.9$), rectangle the POM shallow profile ($a = -2.0$), and triangle the POM deep profile ($a = -0.4$). Double circle represents the control case (experiment 1).

face and the deep water increases with an increase of the rain ratio as seen in Figure 20(a, b, c).

The results of experiment 4 (calcite shallow profile, Figure 20e), experiment 1 (calcite control profile, Figure 20b), and experiment 5 (calcite deep profile, Figure 20d) are roughly compared with the observation (Figure 20f), as the values of d and R in these cases are obtained by fitting the contrast of alkalinity between the surface and the deep water, respectively. However, the slope of alkalinity against total CO_2 in the deep water in each case is different from the others. The slope of the deep water reflects the ratio of calcite remineralization against POM remineralization. For the calcite shallow profile, the range of alkalinity in the deep water is smallest among the three profiles, and the slope of alkalinity against total CO_2 is also smallest. On the other hand, both of the range and the slope for the calcite deep profile are largest. As clearly seen in Figure 20, both of the range and the slope for the calcite control profile are well compared with the observation.

In this way, the optimal estimate of d and R can be determined by comparing various results in our model with the observations. The optimal estimate of the rain ratio R is 0.06 to approximately 0.08. This value coincides with the value estimated by using our two-box model in section 3, which is about 0.06.

Thus, the optimal estimate of four parameters are $a = -0.9$, $r = 0.8\text{yr}^{-1}$, $d = 3500\text{m}$, and $R = 0.08$, respectively. The distributions of other chemical tracers, such as dissolved oxygen, total CO_2, and alkalinity, are well compared with the observation only when the optimal parameter values are used in the model.

6. Conclusion and Remarks

The realistic distributions of tracers have been reproduced by using a biogeochemical general circulation model (B-GCM). The depth of the phosphate maximum

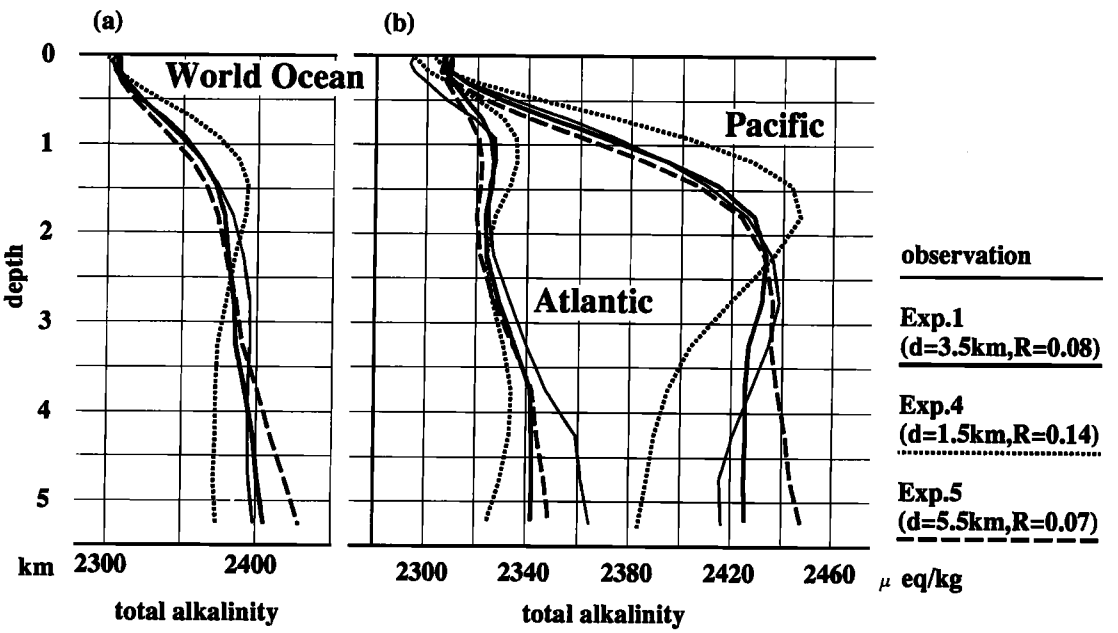

Figure 18. Horizontally averaged vertical profiles of alkalinity at the GEOSECS locations (a) in the world ocean and (b) in the Atlantic and the Pacific. Thick solid lines, thick dotted lines, and thick dashed lines are for the results in experiment 1 (calcite control profile), experiment 4 (calcite shallow profile), and experiment 5 (calcite shallow profile), respectively. Thin solid lines are for the GEOSECS observations.

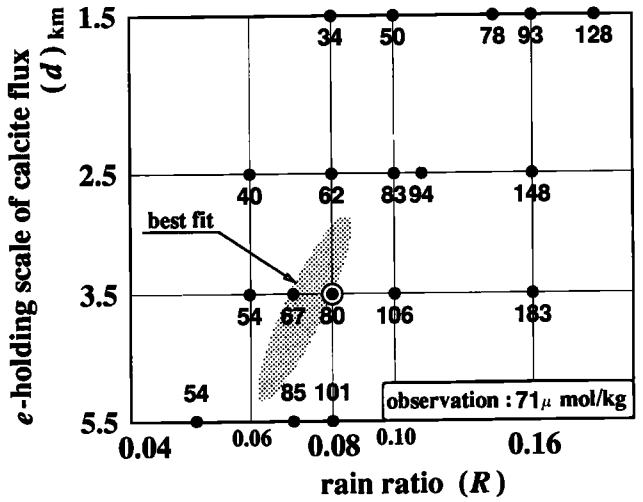

Figure 19. Horizontally averaged difference of alkalinity between the surface and the deep water at GEOSECS locations in the world ocean in the cases changing the rain ratio R and e-holding length scale of calcite vertical flux d. The alkalinity in the surface water is that at the depth of 25m. The alkalinity in the deep water is that vertically averaged over the depths of 1600 to 5500m. Shaded area represents the best fit to the observation. Double circle represents the control case (experiment 1).

in the Atlantic and the Pacific is well compared with the observation. Especially, the observed phosphate maximum in the northern part of the North Pacific is well reproduced by our model.

The difference in the concentrations of tracers between the surface and the deep water depends not only on the export production but also on the remineralization depth. The vertical profile of POM downward flux affects not only the vertical contrast of concentration of tracers between the surface and the deep water, but also on the horizontal contrast within the deep water.

The phosphate distribution depends only on two parameters, the exponent of POC flux a and the bioproduction efficiency r. These values have been determined by comparing the vertical and horizontal phosphate distributions in our model with the observation. The optimal estimates of a and r are -0.9 and 0.8yr^{-1}, respectively. The phosphate distribution can be reproduced only when the profile of POM flux observed by sediment traps is used. The export production is estimated to be about 10 GtC/yr, which is consistent with the observed distribution of phosphate. With determined a and r, the distributions of the chemical tracers except alkalinity are automatically determined in our model, and the alkalinity distribution depends only on two parameters, the e-holding length scale of calcite flux d and the rain ratio R. These values have be also determined by

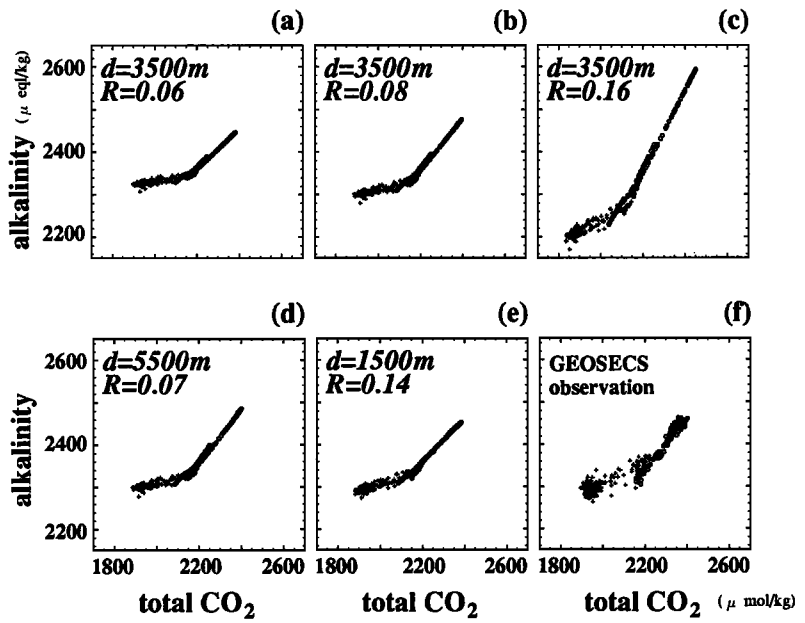

Figure 20. Alkalinity and total CO_2 in the surface and the deep water at the GEOSECS locations in the world ocean: (a) the rain ratio R =0.06 and e-holding length scale of calcite flux d = 3500m (experiment 15), (b) R =0.08 and d = 3500m (experiment 1), (c) R =0.16 and d = 3500m (experiment 18), (d) R =0.07 and d = 5500m (experiment 5), (e) R =0.14 and d = 1500m (experiment 4), and (f) GEOSECS observation. Plus sign represents the surface water (0 to 50m depths) and circle represents the deep water (2500 to 3000m depths). Total CO_2 and alkalinity both in our model results and the observation are normalized by salinity of 35psu.

comparing the vertical and horizontal alkalinity distributions in our model with the observation. The optimal estimates of d and R are 3500m and 0.06 to approximately 0.08, respectively. The determined vertical profile of calcite downward flux is consistent with the data observed by *Anderson and Sarmiento* [1994]. When the carbonate sedimentation on the deep seafloor is taken into account, we found that the value of the rain ratio in the real ocean is expected to be 0.08 to approximately 0.10, which is consistent with the recent observation by *Takahashi et al.* [1990]. The classical value of the rain ratio (= 0.25) should be modified by taking into account the difference of the average remineralization depth between POC and calcite.

Our conclusion that the phosphate distribution can be reproduced by using the profile of POM flux observed by the sediment trap is different from *Najjar et al.* [1992]. This difference is probably due to the difference in circulation field. As shown Figure 15a, the depth of thermocline in our model is much closer to the observation compared with that in their model [*Toggweiler et al.*, 1989]. In fact, *Matear and Holloway* [1995] suggested that the result of the model with only POM transport is consistent with the observed phosphate distribution when only a small modification is made on the circulation field of the Hamburg LSG model. However, in order to simulate more realistic tracer distributions, we should further improve our circulation field, which is a physical oceanographic problem.

Manabe and Stouffer [1993] suggest that the ocean circulation will drastically change owing to global warming when atmospheric CO_2 level becomes 4 times larger than the present one. In such a case, only a B-GCM can predict the distribution of tracers even when the ocean circulation may change from the present state. How will it affect the carbon cycle in the ocean? Will the carbon cycle provide a negative feedback mechanism against climate change? We should answer these questions in the future by using the biogeochemical general circulation model.

Appendix: Treatment of ^{13}C in Our Model

In the gas exchange process (Figure A1), gas exchange rate is controlled by diffusion in the boundary layer at the air-sea interface [*Broecker and Peng*, 1982]. In the following discussion, we assume $^{13}R \equiv {}^{13}C/C \simeq {}^{13}C/{}^{12}C$, which is considered to be a good approximation [*Keeling*, 1981].

Gas exchange between the atmospheric CO_2 and CO_2(aq) at the top of the boundary layer is faster than diffusion within the boundary layer. Therefore we can assume a dissolution equilibrium. A relationship between concentration of atmospheric CO_2 (= C_a) and that of CO_2(aq) at the top of diffusion layer (= C_o) is expressed as,

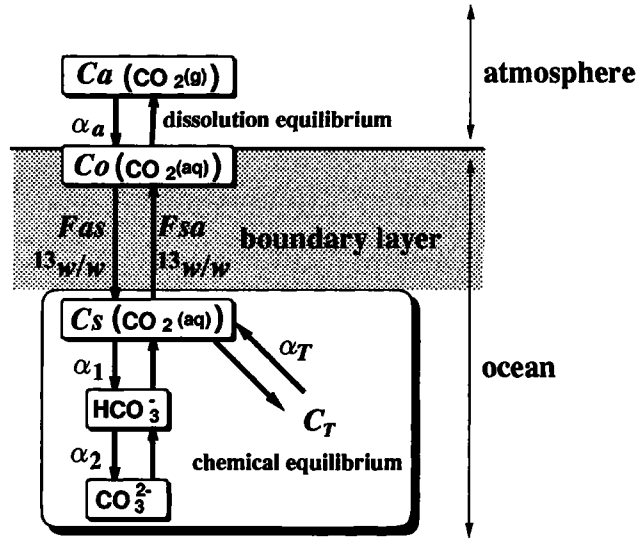

Figure A1. Schematic diagram of gas exchange for CO_2. The α represents a fractionation factor of ^{13}C to ^{12}C.

$$C_o = K_a C_a, \tag{A1}$$

where K_a represents an apparent solubility constant. In the ocean, CO_2, HCO_3^-, and CO_3^{2-} are in the chemical equilibrium. When the alkalinity, temperature, and salinity are given, concentration of CO_2(aq) at the bottom of the boundary layer (= C_S) can be expressed by concentration of total CO_2 (= C_T) as

$$C_S = K_T C_T, \tag{A2}$$

where a coefficient K_T is determined by solving the chemical equilibrium as a function of alkalinity, total CO_2, temperature, and salinity. A net exchange flux of CO_2 from the atmosphere to the ocean can be written as

$$F = F_{as} - F_{sa} = w(C_o - C_S) = w(K_a C_a - K_T C_T), \tag{A3}$$

where w represents a piston velocity for CO_2 gas exchange. Similarly, a net exchange flux of $^{13}CO_2$ can be written as

$$\begin{aligned} F &= {}^{13}F_{as} - {}^{13}F_{sa} \\ &= {}^{13}w\,{}^{13}C_o - {}^{13}w\,{}^{13}C_S \\ &= {}^{13}w\alpha_a K_a\,{}^{13}C_a - {}^{13}w\alpha_T K_T\,{}^{13}C_T \\ &= \alpha_a \frac{{}^{13}w}{w}(wK_aC_a)\frac{{}^{13}C_a}{C_a} - \alpha_T \frac{{}^{13}w}{w}(wK_TC_T)\frac{{}^{13}C_T}{C_T} \\ &\equiv \alpha_{as}F_{as}\,{}^{13}R_a - \alpha_{sa}F_{sa}\,{}^{13}R_T, \end{aligned} \tag{A4}$$

where ^{13}w is a piston velocity for $^{13}CO_2$ gas exchange, α_a represents a fractionation factor for dissolution equilibrium, α_T represents a fractionation factor for the chemical equilibrium between CO_2, HCO_3^- and CO_3^{2-}, $^{13}R_a$ is $^{13}C/^{12}C$ of atmospheric CO_2, and $^{13}R_T$ is $^{13}C/^{12}C$ of total CO_2. Also, α_{as} and α_{sa} represent one-way fractionation factors, which are defined as follows:

$$\alpha_{as} \equiv \alpha_a \frac{^{13}w}{w}, \quad \text{(A5)}$$

$$\alpha_{sa} \equiv \alpha_T \frac{^{13}w}{w}. \quad \text{(A6)}$$

A relation between the piston velocity $^{13}w/w$ and the diffusion coefficient $^{13}D/D$ depends on a presumed gas exchange model. For example, it is represented by $w \propto \sqrt{D}$ for the film replacement model, or $w \propto D$ for the stagnant film model [*Broecker and Peng*, 1982]. A ratio of diffusion coefficient of ^{13}C to ^{12}C is $^{13}D/^{12}D = 0.9991$ [*Schönleber*, 1976; see *Siegenthaler and Münnich*, 1981]. According to *Siegenthaler and Münnich* [1981], we assume that a ratio of piston velocity of ^{13}C to that of ^{12}C is

$$\frac{^{13}w}{w} = 0.9991. \quad \text{(A7)}$$

The temperature dependencies of fractionation factors are

$$\alpha_a = \frac{(^{13}C/^{12}C)_{CO_2(aq)}}{(^{13}C/^{12}C)_{CO_2(g)}} = 0.19 - 0.373\frac{10^3}{T} \text{ ‰} \quad \text{(A8)}$$

$$\alpha_1 = \frac{(^{13}C/^{12}C)_{CO_2(aq)}}{(^{13}C/^{12}C)_{HCO_3^-}} = 24.12 - 9.866\frac{10^3}{T} \text{‰} \quad \text{(A9)}$$

$$\alpha_2 = \frac{(^{13}C/^{12}C)_{CO_2(aq)}}{(^{13}C/^{12}C)_{CO_3^{2-}}} = -7.1 \text{ ‰}, \quad \text{(A10)}$$

which are taken from *Mook et al.* [1974] and *Siegenthaler and Münnich* [1981]. Therefore, α_T is

$$\alpha_T = \frac{[CO_2] + \alpha_1[HCO_3^-] + \alpha_2[CO_3^{2-}]}{[CO_2] + [HCO_3^-] + [CO_3^{2-}]}. \quad \text{(A11)}$$

In this way when alkalinity, temperature, and salinity are given, α_{as} and α_{sa} can be calculated. For example, $\alpha_{as} = -2.0$‰ and $\alpha_{sa} = -10.4$‰ are obtained for the global sea surface average conditions of $T = 18$°C and $S = 35$psu. Similarly, fluxes of $^{13}F_{as}$ and $^{13}F_{as}$ are also calculated under given conditions.

Acknowledgments. We would like to thank Nobuo Suginohara for his helpful discussion and encouragements, and also his critical reading of the manuscript. We would also like to thank Taro Takahashi for his comments and his kindness for giving us his data. The discussion with Jorge L. Sarmiento on the rain ratio and vertical profile of calcite flux was very useful for improving this paper. The comments of the anonymous reviewer particularly on the comparison of our model results with the observations were very helpful. Thanks are extended to Ryuji Tada, Katsumi Hirose, Shinichiro Noriki, Yoshiyuki Nozaki, Syukuro Manabe, and the members of paleoclimate colloquium for their helpful discussions and comments. Numerical calculations were performed by HITAC M-3800 at the Computer Center of the University of Tokyo. Figures were produced by GFD-Dennou Libraries on SUN Microsystems SS2.

References

Anderson, L.A., and J.L. Sarmiento, Redfield ratios of remineralization determined by nutrient data analysis, *Global Biogeochem. Cycles, 8*, 65-80, 1994.

Bacastow, R., and E. Maier-Reimer, Ocean-circulation model of the carbon cycle, *Clim. Dyn., 4*, 95-125, 1990.

Broecker, W.S., and T.-H. Peng, *Tracers in the Sea*, Lamont-Doherty Geological Observatory, Palisades, New York, 1982.

Broecker, W.S., and T.-H. Peng, Interhemispheric transport of carbon dioxide by ocean circulation, *Nature, 356*, 587-589, 1992.

Bryan, F., Parameter sensitivity of primitive general circulation models, *J. Phys. Oceanogr., 17*, 970-985, 1987.

Bryan, K., A numerical method for the study of the circulation of the world ocean, *J. Comput. Phys., 4*, 347-376, 1969.

Craig, H., W.S. Broecker, and S. Spenser, *GEOSECS Pacific Expedition*, vol.4, *Hydrographic Data, 1973-1974*, U.S. Government Printing Office, Washington, D.C., 1981.

Dickson, A.G., and F.J. Millero, A comparison of the equilibrium constants for the dissociation of carbonic acid in sea water media, *Deep Sea Res., 34*, 1733-1743, 1987.

Dickson, A.G., and J.P. Riley, The estimation of acid dissociation constants in seawater media from potentiometric titrations with strong base, I, The ionic product of water (K_w)., *Mar. Chem., 7*, 89-99, 1979.

England, M.H., Representing the global-scale water masses in ocean general circulation models, *J. Phys. Oceanogr., 23*, 1523-1560, 1993.

Eppley, R.W., History, methods, problems, in *Productivity of Ocean: Present and Past*, edited by V.S. Smetacek, G. Wefer, and W.H. Berger, pp.85-97, John Wiley, New York, 1989.

Johansson, O., and M. Wedborg, On the evaluation of potentiomatric titrations of seawater with hydrochloric acid., *Oceanol. Acta, 5*, 209-218, 1979.

Keeling, C.D., The modeling of rare isotopic carbon with regard to notations, in *Carbon Cycle modeling in Scope*, vol.16, edited by B. Bolin, pp.89-94, John Wiley, New York, 1981.

Kroopnick, P.M., The distribution of ^{13}C of ΣCO_2 in the world oceans, *Deep Sea Res., 32*, 57-84, 1985.

Kuo, H., and G. Veronis., Disribution of tracers in hte deep oceans of the world, *Deep Sea Res., 17*, 29-46, 1970.

Heinze, C., E. Maier-Reimer, and K. Winn, Glacial pCO_2 reduction by the World Ocean: Experiments with the Hamburg carbon cycle model, *Paleoceanogr., 6*, 395-430, 1991.

Hellerman, S., and M. Rosenstein, Normal monthly wind stress over the world ocean with error estimates, *J. Phys. Oceanogr., 13*, 1093-1104, 1983.

Ledwell, J.R., A.J. Watson, and C.S. Law, Evidence for slow mixing across the pycnocline form an open-ocean tracer-release experiment, *Nature, 364*, 701-703, 1993.

Levitus, S., Climatological atlas of the world ocean, *NOAA Prof. Rep. 13*, Natl. Oceanic and Atmos. Admin, Boulder,Colo., 1982.

Levitus, S., M.E. Conktight, J.L. Reid, R.G. Najjar, and A. Mantyla, Distribution of nitrate, phosphate, and silicate in the world oceans preindustrial tracer distributions, *Prog. Oceanogr., 31*, 2445-273, 1993.

Manabe,S., and R.J. Stouffer, Century-scale effects of increased atmospheric CO_2 on the ocean–atmosphere system, *Nature, 364*, 215-218, 1993.

Maier-Reimer, E., Geochemical cycles in an ocean gen-

eral circulation model. preindustrial tracer distributions, *Global Biogeochem. Cycles*, *7*, 645-677, 1993.

Martin, J.H., G.A. Knauer, D.M. Karl, and W.W. Broenkow, VERTEX: Carbon cycling in the northeast Pacific, *Deep Sea Res.*, *34*, 267-285, 1987.

Matear, R.J., and G. Holloway, Modeling the inorganic phosphorus cycle of the North Pacific using an adjoint data assimilation model to assess the role of dissolved organic phosphorus, *Global Biogeochem. Cycles*, *9*, 101-119, 1995.

Mook, W.G., J.C. Bommerson, and W.H. Staverman, Carbon isotope fractionation between dissolved bicarbonate and gaseous carbon dioxide, *Earth Planet. Lett.*, *22*, 169-176, 1974.

Najjar, R.G., J.L. Sarmiento, and J.R. Toggweiler, Downward transport and fate of organic matter in the ocean: Simulations with a General Circulation model, *Global Biogeochem. Cycles*, *6*, 45-76, 1992.

Ostlund, H.G., and M. Stuiver, GEOSECS Pacific radiocarbon, *Radiocarbon*, *22*, 25-53, 1980.

Packard, T.T., M. Denis, and P.L. Garfield, Deep-Ocean metabolic CO_2 production: calculations from ETS activity, *Deep Sea Res.*, *35*, 371-382, 1988.

Rintoul, S.R., South Atlantic Interbasin Exchange, *J. Geophys. Res.*, *96*, 2675-2692, 1991.

Scshönleber,G., Messung der isotopentrennung bei der diffusion von $^{13}CO_2$ und $^{12}CO_2$ in wasser, Diploma thesis,, Institutefir Environmental Physics, Univ. of Heidelberg, 1976.

Siegenthaler, U., and K.O. Münnich, $^{13}C/^{12}C$ fractionation during CO_2 transfer from air to sea, in *Carbon Cycle modeling in Scope*, vol.16, edited by B. Bolin, pp.249-257, John Wiley, New York, 1981.

Siegenthaler, S.U., and J.L. Sarmiento, Atmospheric carbon dioxide and the ocean, *Nature*, *365*, 119-125, 1993.

Stuiver, M., and H.G. Ostlund, GEOSECS Atlantic radiocarbon, *Radiocarbon*, *22*, 1-24, 1980.

Suess, E., Particulate organic carbon flux in the oceans — Surface productivity and oxygen utilization, *Nature*, *288*, 260-263, 1980.

Suginohara, N., S. Aoki, and M. Fukasawa, Comments on "On the importance of vertical resolution in certain oceanic general circulation models", *J. Phys. Oceanogr.*, *21*, 1699-1701, 1991.

Sundquist, E.T., Geological perspectives on carbon dioxide and the carbon cycle, in *The Carbon Cycle and Atmospheric CO_2: Natural Variations Archean to Present*, edited by Sundquist,E.T. and W.S. Broecker, pp.5-59, AGU, Washington,D.C., 1985.

Takahashi, T., W.S. Broecker, and A.E. Bainbridge, The alkalinity and total carbon dioxide concentration in the World Oceans, in *Carbon Cycle modeling in Scope*, vol.16, *edited by B. Bolin, pp.271-286, John Wiley*, New York, 1981.

Takahashi, T., C. Goyet, D.W. Chipman, E. Peltzer, J. Goddard, and P.G. Brewer, Ratio of organic carbon and calcium carbonate productions observed at the JGOFS 47°N-20°W site, (abstract), *JGOFS Rep.*,*7*, pp.76-77, JGOFS North Atlantic Bloom Experiment International Scientific Symposium, SCOR/ICSU, 1990.

Tans, P.P., J.A. Berry, and R.F. Keeling, Oceanic $^{13}C/^{12}C$ Observations: A new window on ocean CO_2 uptake, *Global Biogeochem. Cycles*, *7*, 353-368, 1993.

Tans, P.P., I.Y. Fung, and T. Takahashi, Observational constraints on the global atmospheric CO_2 budget, *Science*, *247*, 1431-1438, 1990.

Toggweiler, J.R., K. Dixon, and K. Bryan, Simulations of radiocarbon in a coarse-resolution world ocean model, 1, Steady state prebomb distributions, *J. Geophys. Res.*, *94*, 8217-8242, 1989.

Tsunogai, S., and S. Noriki, Particulate fluxes of carbonate and organic carbon in the ocean. Is the marine biological activity working as a sink of the atmospheric carbon?, *Tellus*, *43B*, 256-266, 1991.

Yamanaka, Y., Development of ocean biogeochemical general circulation model, Ph.D. thesis, 90pp., Univ. of Tokyo, Tokyo, 1995.

Weiss, R.F., The solubility of nitrogen, oxygen and argon in water and sea water, *Deep Sea Res.*, *17*, 721-735, 1970.

Weiss, R.F., Carbon dioxide in water and seawater: the solubility of non-ideal gas, *Mar. Chem.*, *2*, 203-215, 1974.

E. Tajika, Geological Institute, School of Science, University of Tokyo, Bunkyo-ku, Tokyo, 113, Japan. (e-mail: tajika@geol.s.u-tokyo.ac.jp)

Y. Yamanaka, Center for Climate System Research, University of Tokyo, 4-6-1 Komaba, Meguro-ku, Tokyo, 153, Japan. (e-mail: galapen@ccsr.u-tokyo.ac.jp)

(Received November 16, 1994; revised February 8, 1996; accepted February 27, 1996.)